Nonclassical nucleation and growth of inorganic nanoparticles

Jisoo Lee^{1,2*}, Jiwoong Yang^{1,2*}, Soon Gu Kwon^{1,2} and Taeghwan Hyeon^{1,2}

Abstract | The synthesis of nanoparticles with particular compositions and structures can lead to nanoparticles with notable physicochemical properties, thus promoting their use in various applications. In this area of nanoscience, the focus is shifting from size- and shape-uniform single-component nanoparticles to multicomponent nanoparticles with enhanced performance and/or multifunctionality. With the increasing complexity of synthetic reactions, an understanding of the formation mechanisms of the nanoparticles is needed to enable a systematic synthetic approach. This Review highlights mechanistic studies underlying the synthesis of nanoparticles, with an emphasis on nucleation and growth behaviours that are not expected from classical theories. We discuss the structural properties of nanoclusters that are of a size that bridges molecules and solids. We then describe the role of nanoclusters in the prenucleation process as well as in nonclassical nucleation models. The growth of nanoparticles via the assembly and merging of primary particles is also overviewed. Finally, we present the heterogeneous nucleation mechanisms behind the synthesis of multicomponent nanoparticles.

In the past two decades, a tremendous interest in nanoscience and nanotechnology has promoted a rapid development in the synthesis and characterization of various kinds of nanomaterials1-8. The novel characteristics of these nanomaterials, and the resulting potential for applications, derive from the fact that their properties lie between those of molecules and crystalline solids. As the size of a particle increases from the angstrom to the nanometre and micrometre scale, several fundamental changes occur. The molecular symmetry changes to a crystal lattice with periodic long range order9, discrete energy levels turn into a continuous band structure¹⁰ and electrons confined in the molecular orbitals become delocalized11. Advanced synthetic methods have made it possible to manipulate these changes to develop nanomaterials with designed functionalities. For example, nowadays, routine protocols are available to prepare monodisperse single-component nanoparticles, as well as multicomponent nanoparticles with various shapes and compositions. The impact of nanotechnology has propagated from fundamental nanoscience to many applications, including electronics^{5,12}, photonics^{13,14}, plasmonics^{15,16}, energy conversion and storage¹⁷⁻²⁰, catalysis^{21,22} and biomedical engineering^{23–25}. In turn, the performances of the nanomaterials required for these applications impose new challenges on nanoscience. In particular, there is a gap between the need for purposely designed nanoparticles and our current understanding of their formation mechanism. Until the early 2000s, size

uniformity was the biggest issue in nanoparticle synthesis, because it is critical for the production of ensembles of nanoparticles with homogeneous physicochemical properties^{1,2,4}. At the time, various synthetic protocols for the synthesis of monodisperse nanoparticles were developed by empirical approaches. Nowadays, the synthesis of multicomponent nanoparticles is rapidly gaining importance, motivated by the demand for enhanced performance and/or multifunctionality for various applications²⁶⁻²⁹. However, with increasing reaction complexity, conventional trial-and-error approaches become very inefficient; synthetic methods should instead be based on a clear understanding of the formation mechanism of particles, which has yet to be achieved. Recently, the current state of nanochemistry was described as similar to that of organic chemistry in the early twentieth century, when it was transitioning from an empirical art to a science³⁰. In a similar way, we believe that the development of nanochemistry will become increasingly dependent on fundamental understanding.

The characterization of nanomaterials constitutes both a challenge and an opportunity for chemistry and materials science. Characterization techniques optimized for molecules or solids are often not sufficient to fully characterize nanoparticles, thus a combination of multiple techniques is required³¹. On the other hand, studying the formation mechanisms of nanoparticles can provide unique opportunities to explore the 'forbidden' region of the molecule-to-solid transition, in

Center for Nanoparticle Research, Institute for Basic Science (IBS), Seoul 08826, Republic of Korea. School of Chemical and Biological Engineering and Institute of Chemical Processes, Seoul National University, Seoul 08826, Republic of Korea. These authors contributed equally to this work.

Correspondence to S.G.K. and T.H.

kwonsng1@snu.ac.kr; thyeon@snu.ac.kr

Article number: 16034 doi:10.1038/natrevmats.2016.34 Published online 1 Jun 2016 which molecular chemistry meets solid state science. In this Review, we discuss recent advances in the study of the formation mechanisms at work during nanoparticle synthesis. In its early times, the theory of nucleation and growth of nanoparticles was largely borrowed from classical colloid chemistry. However, with the development of nanochemistry, many nonclassical behaviours were identified, revealing new aspects of crystallization at the nanometre scale.

We summarize the formation mechanisms of nanoparticles by organizing them into four sections. First, stable nanoclusters representing the 'missing link' between molecules and solids are discussed. Second, various nonclassical nucleation models in which the nucleation kinetics is altered by the presence of intermediate species are presented, followed by the growth of nanoparticles via the assembly and merging of primary particles. Last, heterogeneous nucleation models for multicomponent nanoparticles are presented.

Molecule-to-solid transition

Structure of molecular clusters. In the classical crystallization theory, there is a clear boundary dividing a crystal from its monomeric building units. However, in nanoscale materials, it becomes evident that this boundary is not abrupt but rather a broad spectrum that spans intermediate structures between molecules and solids. The study of 'missing links' connecting these two categories aids our understanding of how a molecular structure evolves into a crystal^{33–35}.

Nanoclusters are aggregates of tens to hundreds of atoms. One important characteristic shared by various kinds of nanoclusters, including metals³⁶, polyoxometalates³⁷ and metal chalcogenides³⁸, is the presence of discrete structures consisting of a 'magic number' of atoms with extra stability. For bare metal clusters, the stability of these magic clusters is explained in terms of geometric closed-shell structure³⁹⁻⁴¹. By forming a complete closed shell of close-packed atoms with no vacancies at the surface of symmetric polyhedron shapes (that is, Platonic solids), the clusters reach the maximum structural stability for a certain number of constituting atoms. The next largest cluster can be constructed by depositing another complete layer of atoms on the surface of the cluster, which leads to a discrete increase in the number of atoms in each subsequent magic cluster. A homologous series of cuboctahedron clusters (where the number of atoms, n, in each cluster is written as $n = 10/3K^3 - 5K^2 + 11/3K - 1$. where K is the number of atomic shells)³⁹ is shown as an example in FIG. 1a. These structures have been generally observed in clusters of gold and other platinum group metals. It should be noted that although they have symmetric ordered structures, some magic clusters are non-crystalline. For example, icosahedron and decahedron clusters consist of highly strained face-centred cubic (fcc) subunits, and their five-fold symmetry does not belong to the Bravais lattice system. As a result, further growth of the clusters into crystals requires atomic rearrangements to fulfil the translational symmetry condition.

The development of synthesis and characterization techniques for ligand-passivated metal clusters has allowed a generalization of the geometric closedshell theory, leading to the concept of 'super atoms' (REF. 42), which are clusters that exhibit some of the properties of elemental atoms. For example, the structure of $[Au_{25}(RS)_{19}]^-$, where RS is a thiol ligand, can be described as an Au₁₃ core protected by six Au₂(SR)₃ 'staple' motifs $^{43-48}$ (FIG. 1b). The Au_{13} core corresponds to a closed-shell structure with K=2, which gives the cluster good structural rigidity. In addition, this cluster molecule has a full-shell configuration of electronic energy levels, which is analogous to the electronic configuration of noble gas atoms. Indeed, excluding 18 thiolate gold ions, there are 7 gold atoms donating a valence electron from the 6s¹ orbital, plus one electron from the negative charge of the cluster. These 8 electrons fill the molecular orbitals, so that the overall electron configuration resembles the valence shell of neon, $2s^22p^6$ (REF. 42). The same principle applies to other structures. The structure of Au₁₀₂(p-MBA)₄₄ (p-MBA, p-mercaptobenzoic acid) was reported with atomic precision⁴⁹, and it was shown that, although the geometric structure of Au₁₀₂ clusters is not consistent with the closed-shell model, these clusters have good chemical stability because they satisfy the full electron shell condition with 58 (102 Au - 44 thiolated Au) valence electrons⁵⁰. Notably, not all clusters satisfy either geometric or electronic full-shell conditions, as shown in the case of Au₆₈ clusters, which suggests that other stabilization factors are at work⁵¹.

Size-dependent properties of molecular clusters. An interesting structural evolution from molecules to crystalline solids was reported⁵² for a series of dode-canethiol-passivated Au_n clusters, synthesized with n ranging from 38 to ~520. By standardizing the ligand effect, which can alter the structure of the clusters⁵³, it is possible to monitor the systematic transition of Au_n clusters from a non-fcc to a fcc structure as a function of their size (FIG. 1c). This structural transition occurs in the size range n = 144-187. In the same size range, optical absorption spectra show a transition from a molecule-like discrete electronic structure to a bulk-like localized surface plasmon resonance. Consistently, a molecule-like electronic energy transition in Au_n clusters with n < 144 has been reported⁵⁴⁻⁵⁷.

Similarly, CdSe clusters of various sizes and with a motif of a bulk CdSe structure have been synthe-sized $^{38,58-60}$. For example, three pyramidal CdSe clusters with a zinc blende structure — $[Cd_{35}Se_{20}(O_2CPh)_{30}(H_2N-C_4H_9)_{30}]$, $[Cd_{56}Se_{35}(O_2CPh)_{42}(H_2N-C_4H_9)_{42}]$ and $[Cd_{84}Se_{56}(O_2CPh)_{56}(H_2N-C_4H_9)_{56}]$ — have been reported recently 59 (FIG. 1d). By contrast, $[Cd_{32}Se_{14}(SePh)_{36}(PPh_3)_4]$ clusters have a mixed structure with both zinc blende and wurtzite motifs 38 . When plotted against the cluster size, the optical bandgap of these pyramidal clusters coincides with the extrapolation of the bandgap as a function of the size of CdSe nanoparticles 58,59,61 (FIG. 1d), showing that the size-dependent quantum confinement effect is valid for these clusters. In addition, $(CdSe)_{13}$ clusters exhibit a temperature-dependent change in

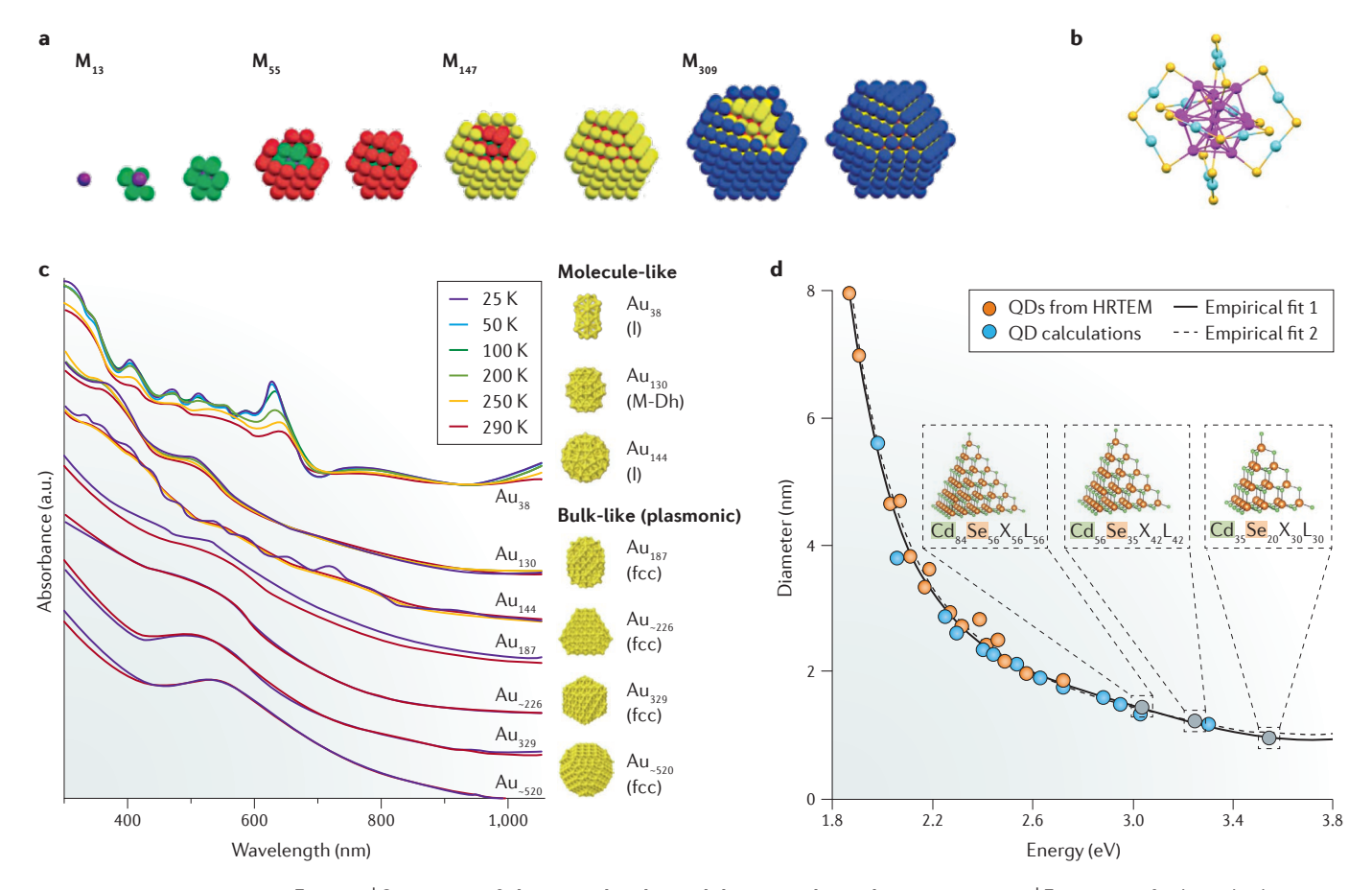


Figure 1 | Structures of cluster molecules and their size-dependent properties. a | Formation of cuboctahedron full-shell clusters. A central atom (purple) is surrounded by close-packed shells of atoms. One-shell (K=2, where K is the number of atomic layers) clusters have 13 atoms and two-shell (K=3) clusters have 55 atoms and so on. **b** | Structure of an Au₂₅RS₁₈ cluster. Sulfur and gold atoms of staple motifs are in yellow and blue, respectively, and the Au₁₃ core is in purple. **c** | Evolution of optical absorption spectra of gold clusters with various sizes, measured at different temperatures, as indicated. Au_n clusters with n=38, 130 and 144 show discrete energy states in the spectra and have icosahedral (l) or Marks decahedral (l)—Oh) structures, whereas the clusters with l=187, ~226, 329 and ~520 have plasmonic resonances originating from their metallic band structure and a face-centred cubic (fcc) structure. **d** | Size dependence of the bandgap energy of CdSe nanoparticles and clusters. The structures of the clusters are shown in the inset and their bandgap energies are indicated as grey dots in the plot. Empirical fit 1 is calculated for data points of both nanoparticles and clusters, whereas empirical fit 2 is for nanoparticles only. The nanoparticle data and empirical fit 2 are from REF. 61. a.u., arbitrary units; HRTEM, high resolution transmission electron microscopy; QDs, quantum dots. Panel **a** is adapted with permission from REF. 43, Royal Society of Chemistry. Panel **b** is adapted with permission from REF. 47, American Chemical Society. Panel **d** is adapted with permission from REF. 59, American Chemical Society.

the bandgap, following Varshini's law, which is the same behaviour as bulk semiconductors⁶². Owing to a low density of states at the band edge, a discrete energy structure is observed not only in semiconductor clusters, but also in nanoparticles of a few nanometres, which is in contrast to what is observed in metal clusters. For this reason, semiconductor nanoparticles are also called 'artificial atoms' (REFS 63,64).

In the case of metal oxides, many clusters that are structurally similar to metal oxide solids were found in polyoxometalate compounds 34,65,66 . Polyoxometalate clusters usually consist of transition metal cations (M) and oxygen atoms surrounding a heteroatom (X), such as Keggin (XM $_{12}O_{40})^{67}$, Wells–Dawson (X $_2M_{18}O_{62})^{68}$ and Anderson (XM $_6O_{24})^{69}$ clusters.

It is interesting to observe that both the expression 'super atoms', for metal clusters, and 'artificial atoms', for semiconducting nanoparticles, can have two meanings. These terms were originally introduced because of the similarity between nanoparticles and atoms, in the sense that both have quantized electronic energy states^{45,64}. This analogy was immediately extended to the other defining property of atoms: that is, that they constitute the building units of bulk solids. In the early days of nanomaterial synthesis, it was suggested that novel metamaterials could be constructed using super atoms and artificial atoms as building blocks^{70,71}. Although the formation of 'artificial molecules' has not yet been fully realized because of the weak quantum exchange coupling between neighbouring artificial atoms^{5,72,73}, the

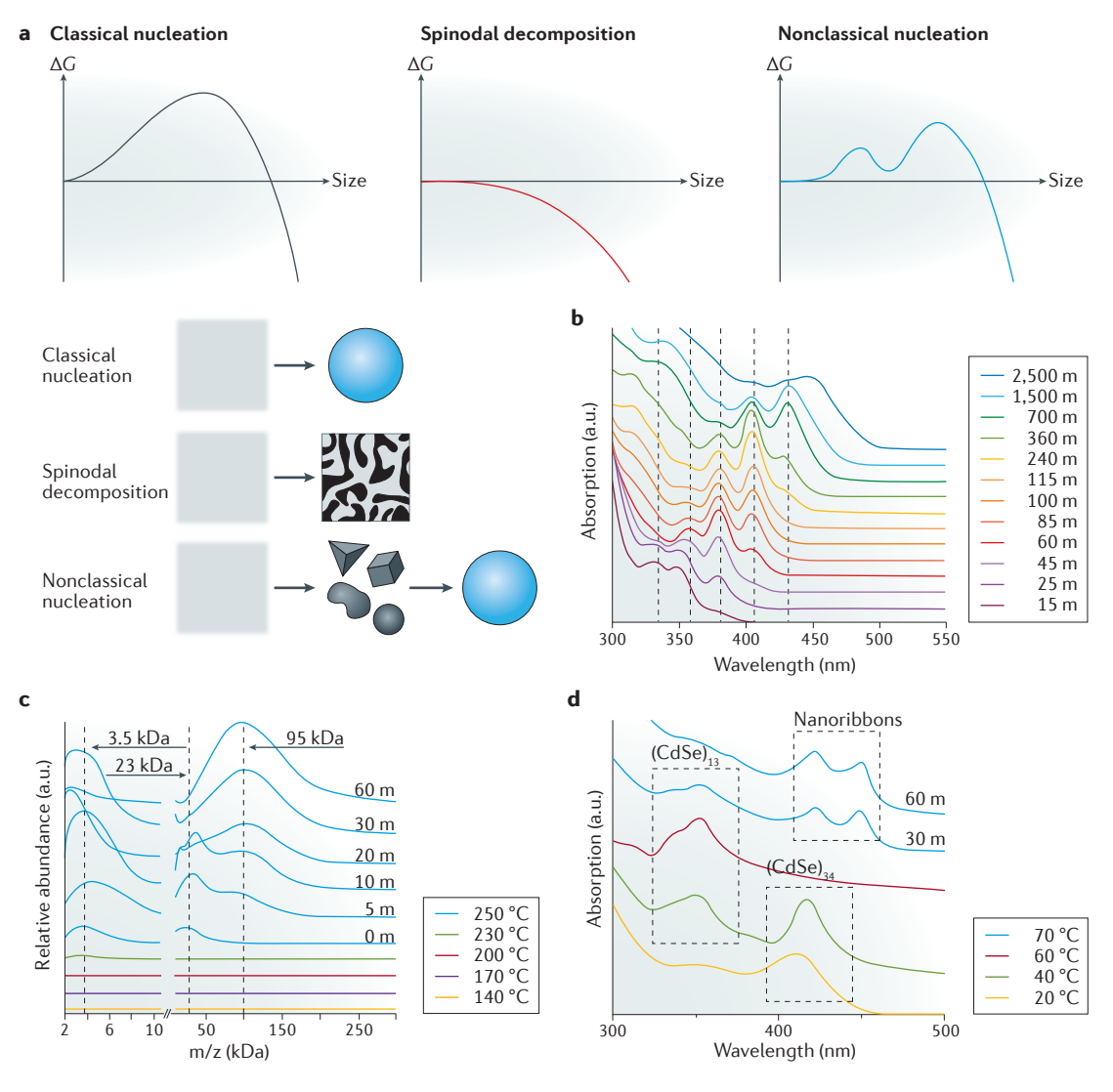


Figure 2 | **Nucleation of colloidal nanocrystals via nonclassical pathways. a** | Plots of free energy change as a function of nucleus size in the classical nucleation (left), spinodal decomposition (middle) and nonclassical nucleation (right) models. **b** | Time dependency of absorption spectra of the reaction mixture during the synthesis of CdSe nanoparticles. Vertical lines indicate absorption peaks corresponding to discrete magic-sized CdSe clusters. **c** | Mass spectra of the reaction mixture during the synthesis of iron oxide nanoparticles. Two different mass ranges are selected for clarity. The peaks at 3.5 kDa, 23 kDa and 95 kDa are attributed to Fe_8 (oleate)₁₁ clusters and to 1.9 nm and 3.3 nm nanoparticles, respectively. **d** | Absorption spectra from the reaction mixture during the synthesis of CdSe nanoribbons. The larger (CdSe)₃₄ clusters are observed before the smaller (CdSe)₁₃ clusters. a.u., arbitrary units; Da, dalton; m/z, mass-to-charge ratio. Panel **b** is adapted with permission from REF. 88, Wiley. Panel **c** is adapted with permission from REF. 95, American Chemical Society. Panel **d** is from REF. 102, Nature Publishing Group.

idea of using clusters and nanoparticles as the building units of solids has contributed to the study of nonclassical crystallization, in which crystal formation proceeds not by the addition of individual atoms or ions but by the assembly of clusters or nanoparticles^{74,75}. The role of clusters and nanoparticles as building units in the nucleation and growth process is discussed in the next two sections.

Prenucleation and nucleation periods

Nucleation is the beginning of condensation and is one of the most ubiquitous phenomena in the universe: stars and planets condense from the interstellar medium⁷⁶, clouds and rain drops condense from water

vapour, and nanoparticles condense from supersaturated solutions. If the condensed phase is crystalline, nucleation is not only accompanied by an abrupt increase in local density, but it also causes an increase in local order. Therefore, the study of nucleation processes can shed light on the general tendency towards self-organization in nature⁷⁷.

In solution, there are three possible nucleation models: classical nucleation, spinodal decomposition and nonclassical nucleation^{75,78} (FIG. 2a). In the classical nucleation theory, homogeneous nucleation has a high thermodynamic energy barrier that originates from the high surface-to-volume ratio of the nucleus. Given that

the surface energy per area, γ , and the bulk energy per volume, ΔG_{γ} , are constant, the free energy change, ΔG , resulting from homogeneous nucleation is written as

$$\Delta G_{\text{hom}}(r) = 4\pi r^2 \gamma + 4/3\pi r^3 \Delta G_{\text{v}} \tag{1}$$

where r is the radius of a spherical nucleus⁷⁹. From the condition d[$\Delta G_{hom}(r)$]/dr=0, the critical radius, $r^* = -2\gamma/\Delta G_{s,r}$ is derived. Only the nuclei with $r \ge r^*$ can spontaneously grow into larger particles $(d[\Delta G_{hom}(r)]/dr < 0)$, whereas those with $r < r^*$ will dissolve in the solution. This energy barrier is important in the synthesis of uniformly sized nanoparticles because it suppresses the random formation of particles in the course of the reaction and induces short bursts of nucleation under high supersaturation^{80,81}. By contrast, spinodal decomposition has practically no energy barrier⁸². In this model, the surface energy of the nuclei is negligible compared with their bulk free energy83, thus spinodal decomposition can spontaneously occur and a phase separation takes place all over the reaction medium. The energetics of nonclassical nucleation are somewhere in between these two extremes of high energy barrier and no barrier 30,84,85. In nonclassical nucleation, unlike what is assumed in classical nucleation theory, γ and ΔG_{v} are not constant with respect to particle size. Instead, there are intermediate structures with lower surface and/or bulk energy, which provide alternative pathways to circumvent the high energy barrier of homogeneous nucleation.

Nonclassical nucleation. It is well known that nanoclusters with discrete sizes and structures form during the prenucleation period of the synthesis of nanoparticles of various metals^{86,87}, semiconductors⁸⁸⁻⁹⁴ and metal oxides^{95,96} (FIG. 2b,c). The formation of these nanoclusters reveals the presence of local minima in the energy landscape, which can effectively lower the energy barrier for nucleation, so that it can take place at a level of supersaturation lower than that estimated by classical nucleation theory 97,98. The relationship between the nanoclusters observed during the nanoparticle synthesis and magicsized clusters has been long recognized 60,99,100. In effect, the magic-sized clusters discussed in the previous section can be regarded as special cases of the transition structures bridging molecules and solids, in the sense that they are thermodynamically stable enough for purification and analysis. Other nanoclusters formed during nanoparticle synthesis are metastable and exist transiently before growing into nanoparticles, making them difficult to characterize. Interestingly, the formation of prenucleation clusters does not always proceed from the smaller to the larger ones. For example, in the early stage of CdSe nanoribbon synthesis, alkylamine-passivated (CdSe)₃₄ clusters are transiently observed before the smaller (CdSe)₁₃ clusters^{62,101,102} (FIG. 2d). This example suggests that the energetics of prenucleation clusters is much more complicated than the picture given in the classical nucleation model.

Stepwise phase transitions. In addition to the geometric full-shell and electronic superatom configurations, which require specific conditions in terms of the number

of atoms and electrons, other structural properties can stabilize prenucleation clusters, resulting in a decrease of the classical nucleation energy barrier. In particular, structural variances, such as amorphism and polymorphism, can contribute to the nonclassical nucleation pathway. Model studies of the 2D crystallization of colloidal microparticles and numerical simulations show that, under low supersaturation conditions, two-step nucleation through an amorphous-to-crystalline transition is energetically favoured over direct crystallization (classical nucleation)^{103–107} (FIG. 3a). In the first step, amorphous nuclei are formed — their surface energy is lower than that of crystalline nuclei as a consequence of their disordered interfaces with the solution. In the second step, an amorphous-to-crystalline transition takes place in the middle of the amorphous phase; this transition has to overcome a much lower free energy barrier compared with direct crystallization from solution. In other words, the amorphous phase can mediate the nucleation of the crystalline phase by buffering the large entropy difference between solution and crystal. Similarly, a twostep nucleation mechanism has been observed in protein crystallization, in which crystalline nuclei are formed inside a metastable dense liquid phase108.

Stepwise phase transitions in the crystallization of polymorphic solids can also induce nonclassical nucleation¹⁰⁹⁻¹¹¹. In equation (1), when the particle is very small $(r << -3\gamma/\Delta G_{v})$, its free energy is dominated by the surface energy term $(4\pi r^2 y)$. On the other hand, as the size of the particle increases, its thermodynamic stability becomes more dependent on the bulk free energy term $(4/3\pi r^3\Delta G_a)$. As a result, in the initial stages, the nucleus tends to have the structure with the lowest surface energy but is transformed to the structure with the lowest bulk free energy as it grows, as conjectured in the Ostwald step rule¹¹². For example, ZrO, nanoparticles have a tetragonal structure, whereas bulk ZrO2 is monoclinic under ambient conditions^{113,114}. A stepwise phase transition occurring because of the difference between the surface and bulk energies of the two phases is illustrated in FIG. 3b. The chemical potential function, $\Delta \mu(r)$, shown in the figure is derived from equation (1) using the relationship $\Delta \mu = [d(\Delta G_{hom})/dV] \times V_m$, where V_m is the molar volume and $\Delta \mu^{\circ} = \Delta G_{v} \times V_{m}$. When the particle radius is smaller than a value r_i , phase 1, which has the lower surface energy (γ_1) , is energetically favoured. However, as the size increases above r_{i} , a phase transition takes place at the cross point indicated by the arrow, after which phase 2, with lower bulk energy ($\Delta \mu_2^{\text{o}}$), becomes more stable. Overall, in nucleation via amorphism and polymorphism, the nuclei are thermodynamically stabilized by their strong tendency to minimize their surface energy.

Structural disorder is observed in various nuclei and very small nanoparticles. In the 1980s, high resolution transmission electron microscopy studies revealed that various metal nanoparticles as small as a few nanometres are in a 'quasi-molten' state, in which their structure and shape are fluctuating from one state to another 40 . It was also theoretically shown that 1.4-nm-sized Au_{55} clusters are more stable in the

amorphous phase than when they form ordered structures¹¹⁵. In 2005, it was reported that the growth of CdSe nanoparticles 2 nm in size, consisting of ~160 atoms, is accompanied by crystallization and shape reconstruction of the nanoparticles, which are initially amorphous¹¹⁶. According to a detailed analysis of the structural disorder in 3.4-nm ZnS and 2-4-nm CdSe nanoparticles using atomic pair distribution function analysis 117,118, these nanoparticles consist of a highly disordered shell and a crystalline core, resembling the crystalline core/amorphous shell structure of the condensed microparticles shown in FIG. 3a. In the synthesis of CdTe nanoparticles with sizes <2 nm, a nucleation energy barrier lower than that expected in the classical model was observed, which is attributed to the 'molten' state of the nanoparticles¹¹⁹. Transmission electron microscopy (TEM) studies of the early stage of the crystallization of minerals, including calcium carbonate, calcium phosphate and iron oxide, indicate that nucleation of these materials is initiated by the formation of amorphous nanoparticles that are transformed into crystalline nanoparticles during growth^{83,97,120-122}. Notably, nucleation from amorphous precursors is commonly observed in biological crystallization, in which cells actively transport and concentrate mineral ions to form the amorphous solid phase from which crystalline nuclei are formed¹²³. Biomimetic model systems, including the polymer-induced liquid-precursor process, show a similar mechanism, in which an amorphous liquid-like phase or a dense liquid phase is formed first, and crystal nucleation takes place within

it¹²⁴. Overall, the formation of amorphous nuclei followed by a stepwise phase transition during growth is commonly observed in various reaction systems.

Aggregation of nuclei. Another important pathway of nonclassical nucleation is aggregation³⁰. Compared with stepwise nucleation, which involves thermodynamic stabilization via structural change, the role of aggregation in the nucleation reaction has a more kinetic origin. As mentioned above, the subcritical nuclei with $r < r^*$ are unstable and supposed to dissolve. However, if their dissolution rate is much slower than their collision rate, it is possible that two or more subcritical nuclei bind together to form a stable post-critical nucleus $(r > r^*)$ before total dissolution. Of course, this process does not only happen for the subcritical nuclei; stable nanoparticles can also aggregate to form larger ones, as we discuss in detail in the following section. Nevertheless, aggregation has a unique role in prenucleation and nucleation periods, because it makes the reaction system deviate far from the classical nucleation model^{84,125,126}. Nucleation is a self-limiting process because the formation of nanoparticles lowers supersaturation and, as the supersaturation level decreases, part of the nuclei disappears by a ripening process⁷⁹. Aggregation can stabilize the nuclei under ripening by abruptly increasing their size, which is equivalent to 'tunnelling' through the free energy barrier — this happens even at low supersaturation, in which growth through atom-by-atom addition to reach the critical radius, r^* , is not possible (FIG. 3c). As

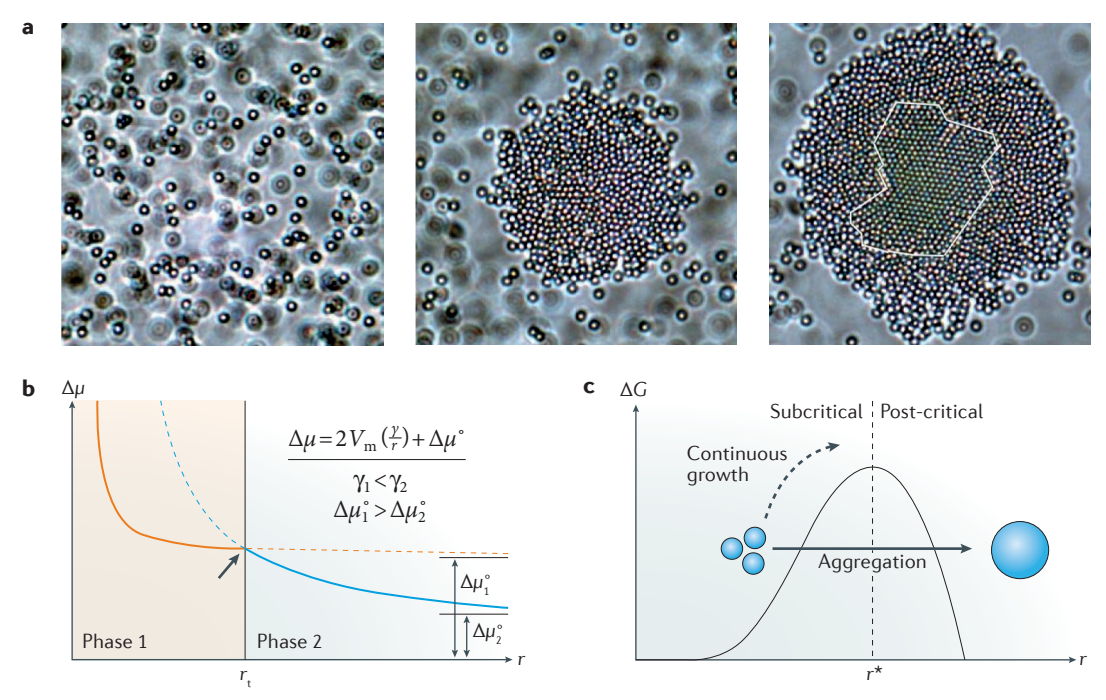


Figure 3 | **Stepwise phase transitions and aggregation of nuclei. a** | Optical microscope images showing the multistep crystallization of colloidal polystyrene particles. A dilute liquid phase is initially observed (left), followed by an amorphous dense phase (middle) and by the formation of crystalline nuclei (right). **b** | Chemical potential plots illustrating the transition from phase 1 (orange curve) to phase 2 (blue curve). **c** | Nucleation by aggregation of prenucleation clusters. r^* , critical radius. Panel **a** is adapted with permission from REF. 103, American Chemical Society.

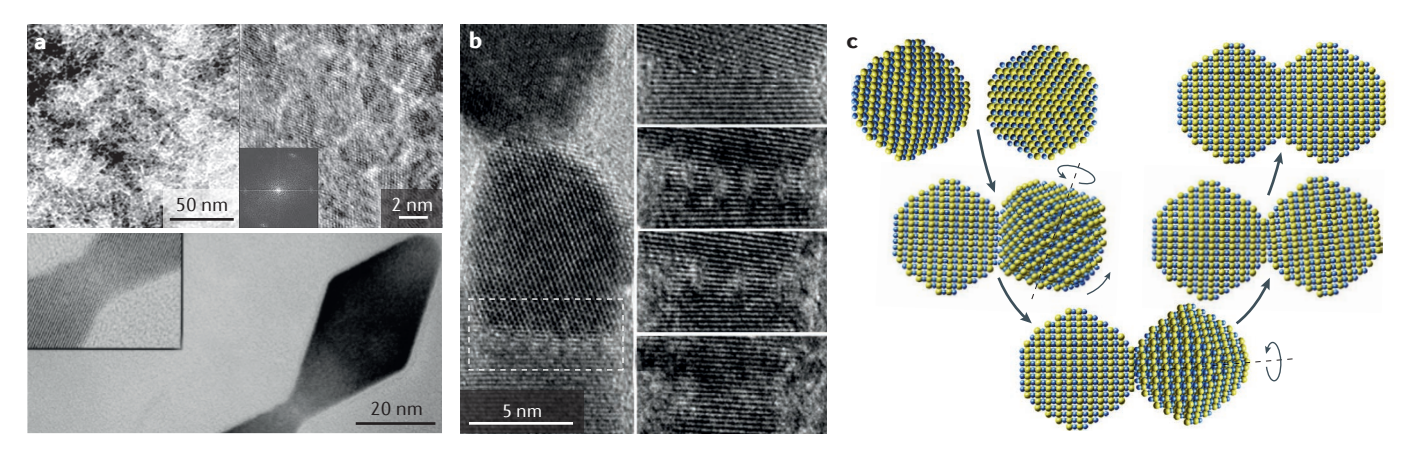


Figure 4 | **Oriented attachment of nanoparticles. a** | Transmission electron microscopy (TEM) image of aggregated ferrihydrite nanoparticles (top). In the inset (right), a domain of aligned nanoparticles is magnified; the fast Fourier transform image shows that the nanoparticles share the same crystallographic axes. A TEM image of oriented attached titania nanoparticles is shown below. **b** | Two attached PbSe nanoparticles with slight lattice misalignment. The lattice structure changes at the interface with passing time from top to bottom (right) — the total intercurring time is 23 minutes. The number of dislocations decreases as the mistilt angle becomes zero; eventually the two particles become a single crystal. **c** | Schematic representation of the rotational motion around three axes that a nanoparticle can perform to align its lattice with that of the nanoparticle it is attached to. Panel **a** is adapted with permission from REF. 142, AAAS, and REF. 145, Elsevier. Panels **b** and **c** are adapted with permission from REF. 152, American Chemical Society.

a result, when the nanoparticle number concentration is high and supersaturation is low, aggregation can be the main nucleation pathway.

The development of liquid-cell TEMs has enabled the direct, real-time in situ observation of the aggregation of nanoparticles in solution 127-132. An in situ measurement shows that the merging of 2 platinum nanoparticles and the subsequent shape reconstruction take place in timescales of hundreds of milliseconds and of less than 20 seconds, respectively 127,130. It was also found that there is a threshold nanoparticle number concentration below which aggregation does not occur¹²⁷. High resolution electron tomography shows further evidence of the aggregation of nuclei $^{51,133-137}$. 3D atomic structures reconstructed using computed tomography reveal that a single metal nanoparticle is made of multiple crystal domains, which originate from the aggregation and merging of smaller nanoparticles in the early stages of the nanoparticle formation process¹³⁶.

In many cases, stepwise nucleation and aggregation work together in a complementary way. Easy formation of amorphous nanoparticles leads to a high number concentration and to more frequent collisions among nanoparticles. Upon aggregation, the small amorphous nanoparticles, because of the abrupt size increase, reach the size regime in which the lower bulk energy is favoured (FIG. 3b), and the amorphous-to-crystalline phase transition takes place. For example, during the precipitation of iron oxide in aqueous solution, amorphous prenucleation clusters of ~2 nm in size are formed first and subsequently aggregate into larger branched network structures83. As the reaction proceeds, crystalline nanoparticles 5-15 nm in size are formed from the denser part of the aggregates. Similar observations were made in the nucleation and growth of calcium phosphate, calcium carbonate and silica 97,120,121,138-140.

Growth by assembly and merging

In classical crystallization theory, crystal growth is described as the addition of atoms or ions to the crystal lattice. This idea is expressed by the change of Gibbs free energy by crystallization, $\Delta G = kT \ln(a/a_0)$, where a and a_0 are the activity of the solute and bulk solid, respectively⁷⁸. In reality, however, this classical model reflects only part of the picture. In the previous section, we discussed how aggregation of prenucleation clusters can contribute to the nucleation process. In a similar way, nanoparticle growth can proceed not only by atom-by-atom addition, but also by the assembly of smaller particles into larger particles^{30,74,75,85,141}. The concept of crystal growth by assembly and merging of primary particles complements the classical theory by extending the definition of the building units from atoms and ions to clusters and nanoparticles. In this section, we examine emerging evidence for nonclassical crystal growth in the synthesis of various nanomaterials and discuss the mechanism behind the nanoparticle assembly and merging processes.

Oriented attachment. Oriented attachment is a well-recognized process for crystal growth from primary nanoparticles ^{142–146}. If two nanoparticles are attached to each other but their crystallographic orientations are not perfectly aligned parallel to each other, defects such as grain boundaries, twinning, or misfit dislocations are formed at the interface^{142,144}. However, in many nanostructures formed by the attachment of primary particles, it was observed that the primary particles are oriented so that they share the same crystal lattice and constitute a single domain^{142,145,147–150} (FIG. 4a). Considering that the probability of two colliding nanoparticles being perfectly oriented by chance is very low, this indicates that the crystal lattices of the nanoparticles become aligned, in some way, during attachment. Recent *in situ* liquid-cell TEM

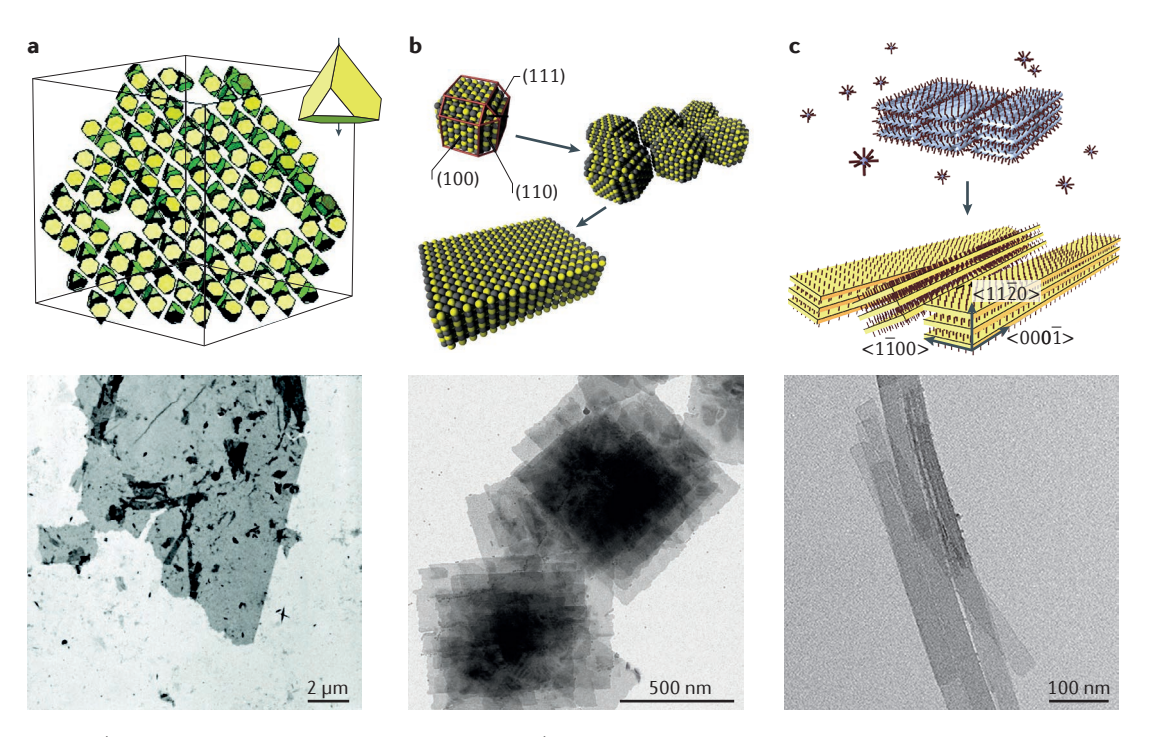


Figure 5 | Formation of 2D nanocrystals by assembly. $\bf a$ | Simulation (top) of the 2D assembly of truncated tetrahedral CdTe nanoparticles, with the electric dipole moment indicated by the arrow and transmission electron microscopy (TEM) image of CdTe nanosheets (bottom). $\bf b$ | Schematic representation (top) and TEM image (bottom) of PbS nanosheets formed by (110) attachment of PbS nanoparticles. $\bf c$ | Schematic illustration showing the transformation of 2D lamellar assembly of (CdSe) $_{13}$ clusters (violet) into CdSe nanoribbons (yellow; top) and TEM image of CdSe nanoribbons (bottom). Panel $\bf a$ is adapted with permission from REF. 161, American Chemical Society. Panel $\bf b$ is adapted with permission from REF. 162, AAAS. Panel $\bf c$ (top) is adapted with permission from REF. 167, American Chemical Society.

studies reveal that there are two underlying mechanisms in the assembly and merging processes (FIG. 4b). First, if two nanoparticles are in close proximity before collision, then there is a strong interaction between them, favouring the alignment of their crystallographic orientations. This interaction is strong enough to induce the rotational and translational motions required to align the nanoparticles before collision. Once the alignment is complete, the nanoparticles immediately merge together by an attractive force^{127,130,146}. For semiconductor nanoparticles, such as CdS, CdTe and ZnS, it was suggested that this mutual alignment is induced by the dipole-dipole interaction between the nanoparticles 148,149,151. However, this theory is not applicable to metal and other nanoparticles that have no permanent dipole moment, and the reason for their alignment has not yet been elucidated127,130. Second, if two misaligned nanoparticles are attached, spontaneous reconstruction of the imperfect lattice takes place during the merging process to remove the defects¹⁴⁶. Even after attachment, the nanoparticles can undergo multiple rotational motions to minimize the misalignment of their lattices¹⁵² (FIG. 4c). These mechanisms show that the thermodynamic driving force for the reduction of the defect-free energy becomes significant at the nanometre scale, where it induces the lattice reconstruction and the motion of the primary particles.

The spontaneous alignment of approaching nanoparticles during oriented attachment reflects the complexity of interparticle interactions at the nanometre scale, which is not fully understood 153,154. In a recent Review article, various nonclassical behaviours of nanoparticle assemblies that are not consistent with the classical theory developed for colloidal microparticles were introduced¹⁵⁵. It was shown that the assumptions made for microparticles to simplify the effects of solvent molecules, non-van der Waals interactions and the particle shape-dependent potentials cannot be extended to nanoparticles. At the nanometre scale, these effects become as important as those produced by the other forces, which makes the interactions between nanoparticles very difficult to analyse. Some interparticle interactions, which are negligibly weak at larger scales, such as the hydrophobic interaction of surface ligands, can have a significant role in nanoparticle assembly 156,157. As a consequence of the complexity of interparticle interactions, nanoparticle self-assembly often leads to unpredictable results, as in the case of quasicrystalline spherical nanoparticle superlattices^{158,159}. Usually, the self-assembly of spherical particles is an entropy-driven process that maximizes space-filling efficiency, which leads to the formation of Bravais lattice structures with translational symmetry. However, quasicrystalline structures have no translational symmetry and cannot be understood in the frame of this entropy model.

In crystal growth by nanoparticle assembly, complex interparticle interactions can result in highly anisotropic nanostructures. Interestingly, different interactions can lead to very similar morphologies, as exemplified by the

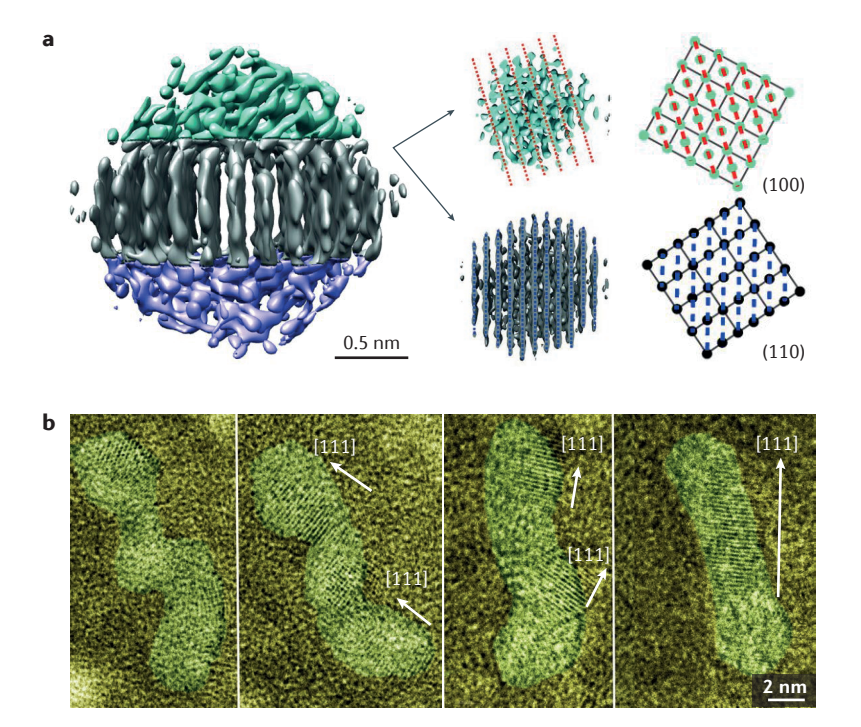


Figure 6 | **Multidomain structures of nanoparticles. a** | Electron tomogram of a face-centred cubic platinum nanoparticle consisting of three domains (left). Cross sectional views of the grain boundary between the upper and the middle domains are shown on the right. The (100) plane of the upper domain and the (110) plane of the middle domain meet with a rotation angle of 14° . The angle is measured with respect to {111} planes, indicated in red and blue dash lines for the upper and middle domain, respectively. **b** | Transmission electron microscopy images show the fusion of three Pt $_3$ Fe particles into a single crystal. From left to right, the crystal orientation changes with atomic redistribution and eventually the crystal shape changes to form a single domain nanorod. Panel **a** is adapted with permission from REF. 131, AAAS.

following three 2D nanostructures with differing compositions. First, it was reported that 3.4-nm-thick CdTe 2D nanosheets are formed by monolayer assembly of the primary CdTe nanoparticles160. In a simulation model study, it was shown that the truncated tetrahedral shape of CdTe nanoparticles and their unidirectional electric dipole moment are determinant for their 2D selfassembly 160,161 (FIG. 5a). Second, in the synthesis of 2.2-nm-thick PbS nanosheets, it was observed that truncated cubic-shaped primary nanoparticles assemble into a nanosheet by preferential attachment of the highly reactive {110} facets, rather than through dipole-dipole interactions^{162,163} (FIG. 5b). Last, another 2D assembly mechanism was revealed in wurtzite CdSe nanostructures 101,102,164,165 that have a fixed thickness of 1.4 nm (FIG. 5c). In this system, ligand-passivated (CdSe)₁₃ clusters assemble into lamellar structures owing to the hydrophobic interaction between the ligands, and then the lamellar cluster assembly structures transform to CdSe nanocrystals^{102,165-169}. Interestingly, zinc blende CdSe nanosheets with thicknesses <2 nm were synthesized using a classical crystal growth process instead of the primary particle assembly 170-173. These examples illustrate the diversity of the nanoparticle assembly behaviours that can be used to build unique nanostructures.

As previously discussed, there is a strong tendency to align the lattices of two nanoparticles upon attachment, but there are some exceptions. Since the 1970s, it has been known that certain specific misalignments or 'twisting' are energetically favoured at the grain boundary of particles in contact^{85,174}. In 2015, the corresponding observation¹³⁶ of grain misalignment at the nanoscale was achieved by electron tomography of platinum nanoparticles smaller than 2 nm (FIG. 6a). The tomogram shows that a single platinum nanoparticle consists of three domains that form twisted grain boundaries. The misalignment is induced to minimize the plane defect free energy at the grain boundary, where the (100) and (110) planes are in contact. The merging of the primary nanoparticles is also accompanied by morphological changes. The attachment of two nanoparticles results in a highly negative surface curvature around the contact point, which makes the structure energetically unstable¹⁷⁵. The surface tension results in a tendency to minimize the net surface area, inducing mass transport to fill the region around the contact point 130. When PbSe nanoparticles are attached through their {100} facets, they are elongated in a direction parallel to their bonding axis to form a 'neck' around their contact point 176. In the unidirectional attachment of Pt₃Fe nanoparticles to form nanorods, a macroscopic reconstruction takes place to straighten the initially rugged surface, as well as to align the lattices of the particles¹³¹ (FIG. 6b). The presence of the surface ligands on the nanoparticles can be an effective barrier for attachment, thus ligand removal is sometimes necessary¹⁷⁷. In addition, it is possible that the mass transport of atoms during merging contributes to the removal of the ligands from the contact region¹⁷⁶. Rather than being totally removed, it was suggested that the ligand molecules are transported by making them 'jump' from one binding site to the next on the surface of the nanoparticle, which requires less energy than desorption178.

Mesocrystals formation. The assembly of primary nanoparticles can also lead to the formation of mesocrystals, in which the nanoparticles remain as individual building units instead of merging into a single crystal domain 74,85,179,180. As a result, mesocrystals have both lattice structures at the atomic scale and secondary structures at the nanometre scale. Mesocrystals are widely observed not only as a result of the assembly of synthesized inorganic nanoparticles, but also in biominerals such as skeletons and shells179. Typically, mesocrystals consist of inorganic nanoparticles and of an organic phase filling the space between the nanoparticles; such unique hybrid structures provide the possibility to control their physicochemical and mechanical properties¹⁸⁰. In addition, mesocrystals can be regarded as intermediate states in the transition from primary nanoparticles to single-domain crystals via assembly and merging 150,181. For this reason, we expect that kinetic studies on the transformation of mesocrystals into single-domain crystals will provide important information on the merging process of primary nanoparticles with different surface ligands and grain boundaries.

In a classical perspective, crystallization is a direct transition from atomic building units to crystals. However, the nucleation and growth processes discussed so far reveal that multiple intermediate steps are involved in the transition¹⁸². In nonclassical pathways, crystallization proceeds from atoms to nanoclusters, to nanoparticles, to mesocrystals, and finally to bulk crystal solids. In this process, the product of each step becomes the building unit for the next, which is characteristic of nonclassical crystallization.

Heterogeneous nucleation

Heterogeneous nucleation takes place in a heterogeneous reaction medium that contains the nucleation seeds. In the synthesis of multicomponent nanoparticles, heterogeneous nucleation is of great importance. By inducing the formation of a secondary phase at the surface of the seed nanoparticles, this process enables the synthesis of a surprisingly wide variety of multicomponent nanostructures^{6,7,26-29,183,184}. However, our current understanding of heterogeneous nucleation at the nanometre scale is far from complete. The mechanism behind the synthetic methods that are based on heterogeneous nucleation is substantially different from that governing the formation of single-component nanoparticles, therefore its study requires new techniques and theoretical frameworks. In this section, we briefly discuss the heterogeneous nucleation theory and examine various nucleation behaviours of multicomponent nanoparticles.

In the heterogeneous nucleation process, a nucleus formed at the surface of a seed can be stabilized by the interface with the seed, which radically changes the energetics of the nucleation reaction compared with that of homogeneous nucleation. To calculate the Gibbs free energy change of heterogeneous nucleation, $\Delta G_{\rm het}$, we assume that a nucleus with a critical radius, r^* , is formed at the surface of a spherical seed with radius R (FIG. 7a). The interface energy, γ_i , of the nucleus and the seed is related to the nucleus–seed contact angle, θ_c , through Young's equation, $\cos\theta_c = (\gamma_s - \gamma_i)/\gamma$, where γ_s and γ are the surface energy of the seed and the nucleus, respectively. The value of $\Delta G_{\rm het}$ can be written 185 as a function of $x = R/r^*$ and $m = \cos\theta_c$ as:

$$\Delta G_{\text{het}} = \frac{8\pi \gamma^3 V_{\text{m}}^2}{3\left[RT \ln \frac{a}{a_0}\right]^2} \times h(m, x)$$
 (2)

where

$$h(m,x) = 1 + \left(\frac{1 - mx}{g}\right)^3 + x^3 \left[2 - 3\left(\frac{x - m}{g}\right) + \left(\frac{x - m}{g}\right)^3\right] + 3mx^2 \left(\frac{x - m}{g} - 1\right)$$
(3)

and $g = \sqrt{1 + x^2 - 2mx} \tag{4}$

When there is no seed (R=0), equation (2) becomes identical to the Gibbs free energy for homogeneous nucleation, $\Delta G_{\text{hom}}(r^*)$ (equation (1)). As the contact angle decreases from 180° (which corresponds to a nucleus and

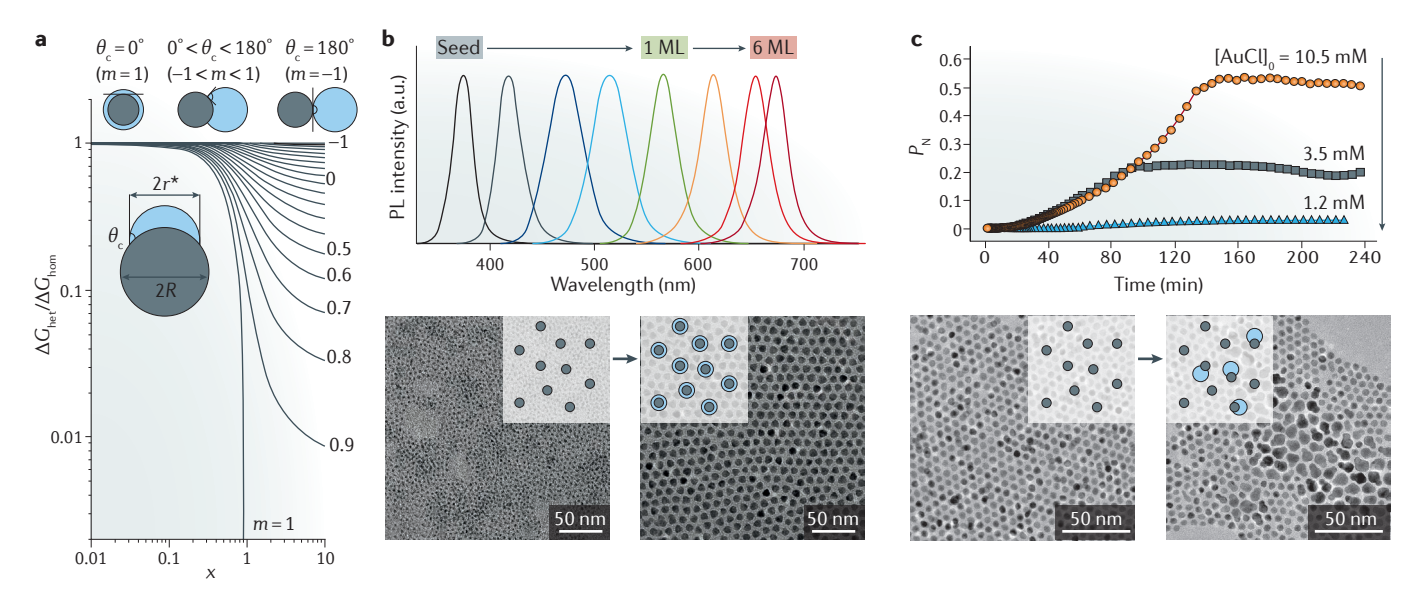


Figure 7 | Energetics and nucleation probability of heterogeneous nucleation. a | Plots of the Gibbs free energy change for heterogeneous nucleation, ΔG_{het} , for a nucleus with a spherical surface of curvature radius r^* . The values of ΔG_{het} calculated from equation (2) are normalized by the Gibbs free energy change for homogenous nucleation, ΔG_{hom} , and plotted against $x = R/r^*$ for various values of $m = \cos\theta_c$, where R is the radius of a spherical seed and θ_c is the contact angle. **b** | Temporal evolution of normalized photoluminescence (PL) spectra of ZnSe–CdSe core–shell nanoparticles during shell formation (top). As the shell thickness increases, the emission peak position is red shifted, whereas the shape and width of the peaks are relatively constant. As the peak shape roughly reflects the size distribution of the nanoparticles (a narrow peak indicates a uniform size distribution), these data indicate the formation of a uniform shell on all seed nanoparticles ¹⁸⁸. Transmission electron microscopy (TEM) images of ZnSe seeds and ZnSe–CdSe core–shells with a shell thickness of 6 monolayers (MLs) (bottom). **c** | Nucleation probability, PN, as a function of reaction time for CoPt₃–Au nanodumbbells synthesized with different concentrations of the gold precursor (AuCl) (top). TEM images of the nanoparticles before and after the reaction of CoPt₃ seeds in a AuCl solution with a concentration of 10.5 mM (bottom). Panel **b** is adapted with permission from REF. 189, American Chemical Society. Panel **c** is from REF. 190, Nature Publishing Group.

seed in contact only at one point), the nucleus becomes more stable with respect to ΔG_{hom} , and eventually the energy barrier goes to 0 when m=1 ($\theta_{\text{c}}=0^{\text{o}}$ is realized when the nucleus envelops the seed, FIG. 7a).

When measuring the heterogeneous nucleation kinetics, it is convenient to use a parameter called nucleation probability, $P_n = N_n/N_{tot}$, where N_n and N_{tot} are the number of seeds that have nuclei and the total number of seeds, respectively 186,187. On the basis of the classical model shown in FIG. 7a, we would expect that the nucleation probability of core-shell nanoparticles, for which the contact angle is 0° (m = 1), is ~100% because the energy barrier for the shell formation is practically 0 due to the low interface energy. This is confirmed by data from the synthesis of semiconductor core-shell nanoparticles^{188,189}. Photoluminescence spectra (FIG. 7b) show that when the seed nanoparticles react in solution with the precursors of the shell material they are all converted into core-shell structures through heterogeneous nucleation and growth of the shell on their surface. By contrast, when the shape of the heterostructures is dumbbell-like, the nucleation probability becomes strongly dependent on the precursor concentration. In the reaction of CoPt₃ seed nanoparticles with a gold precursor, for example, the nucleation probability of CoPt₃-Au nanodumbbells rapidly decreases from 52% to near 0% as the precursor concentration decreases¹⁹⁰ (FIG. 7c). In this case, the interface energy between CoPt, and Au is relatively high, so that the contact angle is larger than 0 (m < 1). As a result, the energy barrier, ΔG_{het} , can effectively block the heterogeneous nucleation and the nuclei can form only on part of the seeds (FIG. 7c). In general, the interface energy is the main factor that determines the shape of the nucleus in heterogeneous nucleation183,184, as well as the height of the energy barrier of the nucleation reaction.

Interface energy minimization and property tuning by lattice strain. In the section on homogeneous nucleation, we mentioned that the tendency to reduce the surface energy results in nonclassical nucleation behaviours. Correspondingly, in heterogeneous nucleation, there is a strong tendency to minimize the interface energy of the nucleus and the seed. If the nucleus and the seed form a heteroepitaxial interface, the interface energy increases with their lattice mismatch. As a result, their lattices are mechanically strained to reduce the mismatch at the interface. For example, in the synthesis of CoPt₃-Au nanodumbbells mentioned above, it was observed that the lattice of the CoPt, seeds is strained by a stress of 2.4 GPa when the gold phase nucleates on their surface¹⁹⁰. This happens because both CoPt₃ and Au have a fcc structure, but their lattice mismatch is 5.3%. For wurtzite CdS-ZnS core-shell nanoparticles, which have a lattice mismatch of 7%, a stress of >4 GPa was observed for shells with a thickness of 7.5 monolayers¹⁹¹. Lattice strain in the overgrowth phase to remove the mismatch with the substrate lattice is commonly observed in heteroepitaxial thin film growth, a phenomenon known as pseudomorphism^{192,193} (FIG. 8a). However, unlike thin film substrates, seed nanoparticles have very small finite sizes, thus the restoration force from the strained

overgrowth phase can induce deformation of the seed, so that the forces in the seed and in the overgrowth phase are in equilibrium (FIG. 8b). As shown in the case of $CoPt_3$ –Au nanodumbbells and CdS–ZnS core–shells, the mechanical stress induced by the formation of a heteroepitaxial interface can be very high. From the synthetic point of view, this behaviour can be exploited to control the lattice of the multicomponent nanoparticles by selecting seeds and overgrowth phases with appropriate lattice mismatch and elastic moduli.

The idea of adjusting the lattice constant to modify the physicochemical properties of nanoparticles has been demonstrated both experimentally and theoretically. In general, lattice strain in semiconductors induces changes in the bandgap energy and in the charge carrier mobility. Using this property, the bandgap offset of semiconductor nanoparticles with heteroepitaxial core-shell structures can be modified194. By encapsulating 'soft' (low elastic modulus) CdTe cores with a shell of other II-VI semiconductors with smaller lattice constants, compressive stress in the core and extensional stress in the shell can be induced simultaneously. As the relative strain in the core and in the shell is determined by the shell thickness, the band alignment can be transformed from type I to type II, as indicated by optical absorption spectra (FIG. 8c). In addition, it was shown by theoretical simulations that the mechanical stress within the core-shell structure can make a high-pressure phase stable at ambient pressure. For example, for bulk CdSe, the rocksalt structure is stable only under a pressure of ~2 GPa. By contrast, in a simulation of CdSe-ZnS coreshell nanoparticles, if the nanoparticle is subjected to a pressure of 20 GPa, the rocksalt CdSe core remains metastable even after the external pressure is removed¹⁹⁵. Similarly, in another simulation model, it was shown that rocksalt CdSe can be stabilized under atmospheric pressure in a ZnS-CdSe-ZnS core-shell-shell structure because of heteroepitaxial lattice strain¹⁹⁶. Lattice tuning is also relevant for the synthesis of nanoparticles with improved electrocatalytic activity. According to density functional theory calculations, there is an optimum lattice strain of platinum that results in enhanced catalytic activity in the oxygen reduction reaction compared with unstrained platinum^{197–199}. A simulation of the catalytic activity of Cu_xPt_(1-x)-Pt core-shell nanostructures, in which the strain was continuously adjustable in the range between -4.5% and 0% by controlling the ratio of copper and platinum in the core¹⁹⁹, is shown in FIG. 8d. It was also experimentally confirmed that Cu–Pt-alloy core/lattice-strained-Pt shell nanoparticles have high catalytic activity compared with pristine platinum nanoparticles¹⁹⁷. A similar approach of lattice strain tuning to enhance the catalytic activity was reported for FePt-Pt core-shell nanoparticles¹⁹⁸.

Obviously, having similar crystal structures is not a necessary condition for heterogeneous nucleation, and there are other ways to lower the interface energy between seeds and nuclei. Among them, the coincidence site lattice model explains the cases in which two different crystal structures have a coherent interface^{200,201}. In FIG. 8e, for example, the (111) planes of γ -Fe,O₃ and

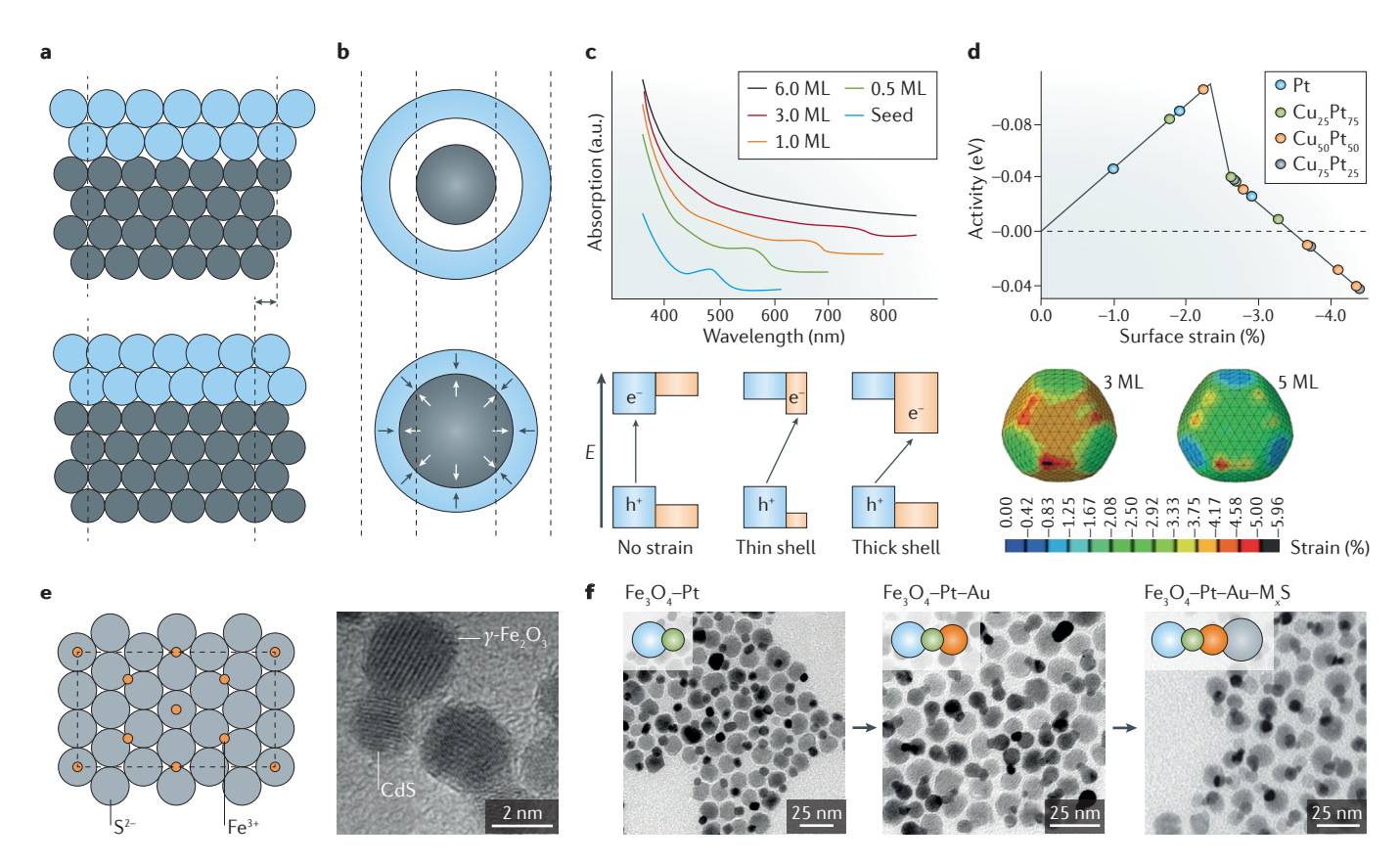


Figure 8 | Lattice strain and structural properties of multicomponent nanoparticles. a | Schematic illustrations of an unstrained overgrowth layer (blue; top) and of a pseudomorphic layer (bottom) on the substrate (grey). b | Unstrained core and shell (top) and strained core–shell structure (bottom). The arrows indicate the direction of the radial stress in the core and in the shell. c | Absorption spectra of CdTe–ZnSe core–shell nanoparticles with different shell thicknesses and corresponding band diagrams. As the shell thickness increases, negative and positive strain is induced in the core and the shell, respectively. This leads to a conversion of the band structure from type I to type II, as illustrated in the sketch below and as indicated by the red shift of the absorption peak position. d | Plot for the catalytic activity of platinum for the oxygen reduction reaction as a function of the surface strain of platinum atoms (top). Circles with different colours show the activity of simulated Cu-Pt/Pt core-shell nanoparticles with a shell thickness of 3–5 monolayers (MLs). Simulation of surface strain for 3 and 5 ML-thick platinum shells on a 5 nm Cu_{so}Pt_{so} core (bottom). **e** | Coincidence site (dashed box) of the interface between the γ -Fe₂O₃(111) and the zinc blende CdS (111) planes. The Fe $^{3+}$ lattice is expanded by 4.6% to remove the mismatch with the S^{2-} lattice. The transmission electron microscopy (TEM) image shows γ -Fe₂O₂-CdS nanodumbbells. \mathbf{f} | Schematic illustrations and TEM images showing sequential synthesis of Pt–Fe $_3$ O $_4$ heterodimers, Pt–Fe $_3$ O $_4$ –Au heterotrimers and Pt–Fe $_3$ O $_4$ –Au–Cu $_6$ S $_5$ heterotetramers. Panel c is from REF. 194, Nature Publishing Group. Panel d is adapted with permission from REF. 199, American Chemical Society. Panel e is adapted with permission from REF. 202, American Chemical Society. Panel f is from REF. 208, Nature Publishing Group.

zinc blende CdS are shown together. Although their 3D structures have little resemblance, the 2D lattices of Fe³+ and S²- on the (111) plane can be overlapped with a small lattice mismatch of 4.6%. As a result, γ -Fe₂O₃-CdS nanodumbbells can be synthesized through the formation of a (111)/(111) interface²0². Note that, since the zinc blende CdS (111) plane and the wurtzite CdS (001) plane are equivalent, wurtzite CdS nanoparticles are also formed via the CdS(001)/ γ -Fe₂O₃(111) interface. An interface of coincidence lattices can be formed not only between well-defined facets, but also between curved surfaces, as exemplified by the formation of γ -Fe₂O₃ nanoparticles at the tip of bent TiO₂ nanorods²0³. High chemical affinity is another important factor that facilitates heterogeneous nucleation. Owing

to the strong chemical bonds between noble metals (gold, silver and platinum) and chalcogens (sulfur, selenium and tellurium), it is easy to induce the deposition of either metals on the surface of chalcogenide nanoparticles or chalcogens on the surface of metal nanoparticles. Using this approach, various nonepitaxial multicomponent nanostructures, including gold-tipped CdSe nanorods 204,205 , Au–CdS core–shell nanoparticles 206 and FePt–CdS nanodumbbells 207 , have been prepared. Furthermore, it was demonstrated that by using chemoselective deposition of metals and metal sulfides, heterotrimers and heterotetramers can be prepared by using Pt–Fe $_3O_4$ nanodumbbells as seeds 208 . As shown in Fig. 8f, if a gold precursor is reacted with Pt–Fe $_3O_4$ heterodimers, gold nanoparticles exclusively nucleate

on the surface of platinum. Then, the reaction of the heterotrimers with metal and sulfur precursors leads to the formation of metal sulfide nanoparticles attached to only gold nanoparticles to form linear heterotetramers.

Finally, it is also reported that coincidence lattices and chemical affinity can work in a complementary way to lead to the formation of low-energy interfaces. In the case of UO_2 – In_2O_3 and FePt– In_2O_3 nanodumbbells, the lattice of In_2O_3 is strained so that the interfaces are coherent ²⁰⁹; however, the preferred nucleation sites on the seeds are not the facets with the minimum lattice mismatch but the ones with the strongest chemical affinity.

Conclusions

The rapid development of nanochemistry has been, so far, largely sustained by knowledge coming from various traditional research areas. In the early times of the field, scientists working in nanochemistry tried to explain their observations using well-established classical theories. For example, many of the synthetic reactions for the formation of nanoparticles were adopted from organometallic and sol-gel chemistry. The main concepts behind the formation mechanisms of monodisperse nanoparticles are direct extensions of the classic theory of colloidal chemistry, such as bursts of nucleation described by the LaMer diagram. Nowadays, as nanochemistry becomes a mature field, nonclassical phenomena that are unique to nanoscale materials are attracting an increasing amount of interest. In this Review, we discussed nucleation and growth mechanisms in nanoparticle synthesis that are not consistent with the classical crystallization theory. As we briefly mentioned in the introduction, the study of nonclassical crystallization of nanoparticles is of pivotal importance to establish a fundamental understanding of nanochemistry and to provide technical solutions for various applications of nanomaterials.

With increasing evidence of nonclassical crystallization behaviours at the nanoscale, the modification of some aspects of the traditional crystallization theory is strongly required. Multistep nucleation and the formation of nanoclusters in the prenucleation period can make the reaction system deviate from the one predicted by classical nucleation theory, which assumes a singlestep transition from solute to solid. At the moment, however, experimental data on the prenucleation and nucleation periods of the nanoparticle formation are still limited, which hampers the development of more realistic theoretical models. Despite the technical difficulties in monitoring sub- and few-nanometre sized objects, a number of significant contributions have been made using *in situ* TEM, X-ray scattering and optical spectroscopy techniques. With the continuous development of characterization techniques, it is expected that more detailed information on the kinetics and on the structural changes in the prenucleation and nucleation periods will be available soon.

The formation of diverse intermediate structures between atoms and crystalline solids, which include nanoclusters, nanoparticles and mesocrystals, changes the traditional view of crystallization. Instead of the direct assembly of atoms into crystalline lattices, the intermediate structures in nonclassical crystallization show various assembly and aggregation behaviours at different scales, from subnanometre up to tens of nanometres. Sometimes those behaviours lead to anisotropic crystal growth or superlattice structure formation, adding much more complexity to crystal structures than what would be expected from classical crystallization theory. We expect that future studies on multiscale assembly mechanisms will give valuable insight into material self-organization, as in the case of biomineralization.

The importance of the synthesis of multicomponent nanoparticles with desired interfaces and morphologies is rapidly increasing due to the technical requirements for applications, such as catalytic activity and efficient charge and mass transport. As mentioned above, nonclassical crystallization studies provide an effective framework for the understanding and control of the structural complexity of nanomaterials. In particular, the study of heterogeneous nucleation mechanisms of multicomponent nanoparticles is needed to understand the energetics of the interface formation and of structural changes during synthesis. We believe that the study of nanochemistry will not only contribute to fundamental science, but will also form the basis of a systematic approach for the synthesis of complex nanostructures with improved performance.

- Murray, C. B., Norris, D. J. & Bawendi, M. G. Synthesis and characterization of nearly monodisperse CdE (E = S, Se, Te) semiconductor nanocrystallites. J. Am. Chem. Soc. 115, 8706–8715 (1993).
- Rogach, A. L. et al. Organization of matter on different size scales: monodisperse nanocrystals and their superstructures. Adv. Funct. Mater. 12, 653–664 (2002).
- Yin, Y. & Alivisatos, A. P. Colloidal nanocrystal synthesis and the organic–inorganic interface. *Nature* 437, 664–670 (2005).
- Park, J., Joo, J., Kwon, S. G., Jang, Y. & Hyeon, T. Synthesis of monodisperse spherical nanocrystals. Angew. Chem. Int. Ed. Engl. 46, 4630–4660 (2007)
- Talapin, D. V., Lee, J. S., Kovalenko, M. V. & Shevchenko, E. V. Prospects of colloidal nanocrystals for electronic and optoelectronic applications. *Chem. Rev.* 110, 389–458 (2010).
- Carbone, L. & Cozzoli, P. D. Colloidal heterostructured nanocrystals: synthesis and growth mechanisms. *Nano Today* 5, 449–493 (2010).

- Donegá, C. d. M. Synthesis and properties of colloidal heteronanocrystals. *Chem. Soc. Rev.* 40, 1512–1546 (2011).
- Kovalenko, M. V. et al. Prospects of nanoscience with nanocrystals. ACS Nano 9, 1012–1057 (2015). This paper provides a broad perspective on the current state of nanoscience and nanoparticle synthesis.
- Cleveland, C. L. et al. Structural evolution of smaller gold nanocrystals: the truncated decahedral motif. Phys. Rev. Lett. 79, 1873–1876 (1997).
- Kubo, R., Kawabata, A. & Kobayashi, S. Électronic properties of small particles. *Annu. Rev. Mater. Sci.* 14, 49–66 (1984).
- Alivisatos, A. P. Semiconductor clusters, nanocrystals, and quantum dots. *Science* 271, 933–937 (1996).
- Kim, J.-Y. & Kotov, N. A. Charge transport dilemma of solution-processed nanomaterials. *Chem. Mater.* 26, 134–152 (2014).
- Shirasaki, Y., Supran, G. J., Bawendi, M. G. & Bulovič, V. Emergence of colloidal quantum-dot light-

- emitting technologies. *Nat. Photonics* **7**, 13–23 (2013).
- Choi, M. K. et al. Wearable red–green–blue quantum dot light-emitting diode array using high-resolution intaglio transfer printing. Nat. Commun. 6, 7149 (2015).
- Atwater, H. A. & Polman, A. Plasmonics for improved photovoltaic devices. *Nat. Mater.* 9, 205–213 (2010).
- Barnes, W. L., Dereux, A. & Ebbesen, T. W. Surface plasmon subwavelength optics. *Nature* 424, 824–830 (2003).
- Carey, G. H. et al. Colloidal quantum dot solar cells. Chem. Rev. 115, 12732–12763 (2015).
- Armand, M. & Tarascon, J. M. Building better batteries. *Nature* **451**, 652–657 (2008).
- Aricò, A. S., Bruce, P., Scrosati, B., Tarascon, J. M. & Schalkwijk, W. V. Nanostructured materials for advanced energy conversion and storage devices. *Nat. Mater.* 4, 366–377 (2005).
- Guo, S., Zhang, S. & Sun, S. Tuning nanoparticle catalysis for the oxygen reduction reaction. *Angew. Chem. Int. Ed. Engl.* 52, 8526–8544 (2013).

RFVIFWS

- Somorjai, G. A. & Park, J. Y. Molecular factors of catalytic selectivity. Angew. Chem. Int. Ed. Engl. 47, 9212-9228 (2008)
- Somorjai, G. A., Contreras, A. M., Montano, M. & Rioux, R. M. Clusters, surfaces, and catalysis. *Proc.* Natl Acad. Sci. USA 103, 10577-10583 (2006).
- Giljohann, D. A. & Mirkin, C. A. Drivers of biodiagnostic development. Nature 462, 461-464 (2009)
- Lee, N. et al. Iron oxide based nanoparticles for multimodal imaging and magnetoresponsive therapy. Chem. Rev. 115, 10637-10689 (2015).
- Medintz, I. L., Uyeda, H. T., Goldman, E. R. & Mattoussi, H. Quantum dot bioconjugates for imaging, labelling and sensing. Nat. Mater. 4, 435-446 (2005).
- Costi, R., Saunders, A. E. & Banin, U. Colloidal hybrid nanostructures: a new type of functional materials Angew. Chem. Int. Ed. Engl. 49, 4878-4897 (2010).
- Goesmann H & Feldmann C Nanoparticulate functional materials. Angew. Chem. Int. Ed. Engl. 49, 1362-1395 (2010).
- Buck, M. R. & Schaak, R. E. Emerging strategies for the total synthesis of inorganic nanostructures. *Angew. Chem. Int. Ed. Engl.* **52**, 6154–6178 (2013). Wang, C., Xu, C., Zeng, H. & Sun, S. Recent progress in
- syntheses and applications of dumbbell-like nanoparticles. Adv. Mater. 21, 3045-3052 (2009).
- Wang, F., Richards, V. N., Shields, S. P. & Buhro, W. E. Kinetics and mechanisms of aggregative nanocrystal growth. *Chem. Mater.* **26**, 5–21 (2014).
- Billinge, S. J. L. The nanostructure problem. *Physics* **3**. 25 (2010).
- Sugimoto, T. Preparation of monodispersed colloidal particles. Adv. Colloid Interfac. Sci. 28, 65-108 (1987).
- Zheng, J., Zhang, C. & Dickson, R. M. Highly fluorescent, water-soluble, size-tunable gold quantum dots. Phys. Rev. Lett. 93, 77402 (2004).
- Sadeghi, O., Zakharov, L. N. & Nyman, M. Aqueous formation and manipulation of the iron-oxo Keggin
- ion. Science **347**, 1359–1362 (2015). Miller, J. S. & Drillon, M. (eds) Magnetism: Molecules to materials III: Nanosized Magnetic Materials (Wiley-
- Schmid, G. Large clusters and colloids. Metals in the embryonic state. *Chem. Rev.* **92**, 1709–1727 (1992). Gatteschi, D., Caneschi, A., Pardi, L. & Sessoli, R.
- Large clusters of metal ions: the transition from molecular to bulk magnets. Science 265, 1054-1058
- Soloviev, V. N., Eichhöfer, A., Fenske, D. & Banin, U. Size-dependent optical spectroscopy of a homologous series of CdSe cluster molecules. J. Am. Chem. Soc. **123**, 2354–2364 (2001).
- Martin, T. P. Shells of atoms. Phys. Rep. 273 199-241 (1996).
- Marks, L. D. Experimental studies of small particle structures. *Rep. Prog. Phys.* **57**, 603–649 (1994). Baletto, F. & Ferrando, R. Structural properties of
- nanoclusters: energetic, thermodynamic, and kinetic effects. Rev. Mod. Phys. 77, 371-423 (2005).
- Häkkinen, H. Atomic and electronic structure of gold clusters: understanding flakes, cages and superatoms from simple concepts. *Chem. Soc. Rev.* **37**, 1847-1859 (2008).
- Schmid, G. The relevance of shape and size of Au₅₅ clusters. *Chem. Soc. Rev.* **37**, 1909–1930 (2008). Heaven, M. W., Dass, A., White, P. S., Holt, K. M. &
- Murray, R. W. Crystal structure of the gold nanoparticle [N(C₈H₁₇)₄][Au₂₅(SCH₂CH₂Ph)₁₈]. *J. Am. Chem. Soc.* **130**, 3754–3755 (2008).
- Akola, J., Walter, M., Whetten, R. L., Häkkinen, H. & Grönbeck, H. On the structure of thiolate-protected Au₂₅. *J. Am. Chem. Soc.* **130**, 3756–3757 (2008). Häkkinen, H. The gold–sulfur interface at the
- nanoscale. Nat. Chem. 4, 443-455 (2012).
- Qian, H., Zhu, M., Wu, Z. & Jin, R. Quantum sized gold nanoclusters with atomic precision. Acc. Chem. Res.
- 45, 1470–1479 (2012). Zhu, M., Aikens, C. M., Hollander, F. J., Schatz, G. C. & Jin, R. Correlating the crystal structure of a thiolprotected Au₂₅ cluster and optical properties. J. Am. Chem. Soc. 130, 5883-5885 (2008).
- Jadzinsky, P. D., Calero, G., Ackerson, C. J. Bushnell, D. A. & Kornberg, R. D. Structure of a thiol monolayer-protected gold nanoparticle at 1.1 Å resolution. Science 318, 430–433 (2007).
- Walter, M. et al. A unified view of ligand-protected gold clusters as superatom complexes. Proc. Natl Acad. Sci. USA 105, 9157-9162 (2008).

- 51. Azubel, M. et al. Electron microscopy of gold nanoparticles at atomic resolution. Science 345 909-912 (2014).
- Negishi, Y. et al. A critical size for emergence of nonbulk electronic and geometric structures in dodecanethiolate-protected Au clusters. J. Am. Chem. Soc. 137, 1206-1212 (2015)
- Cha, S. H., Kim, J. U., Kim, K. H. & Lee, J. C. Preparation and photoluminescent properties of gold(I)-alkanethiolate complexes having highly ordered supramolecular structures. Chem. Mater. 19, 6297-6303 (2007).
- Devadas, M. S. et al. Temperature-dependent optical absorption properties of monolayer-protected Au and Au₃₈ clusters. J. Phys. Chem. Lett. **2**, 2752–2758 (2011).
- Tian, S. et al. Structural isomerism in gold nanoparticles revealed by X-ray crystallography. Nat. Commun. 6, 8667 (2015).
- Parker, J. F., Fields-Zinna, C. A. & Murray, R. W. The story of a monodisperse gold nanoparticle: Au₂₅L₁₈. Acc. Chem. Res. 43, 1289-1296 (2010).
- Xu, W. W. & Gao, Y. Unraveling the atomic structures of the Au₆₈(SR)₃₄ nanoparticles. *J. Phys. Chem. C* **119**, 14224–14229 (2015).
- Soloviev, V. N., Eichhofer, A., Fenske, D. & Banin, U Molecular limit of a bulk semiconductor: size dependence of the "band gap" in CdSe cluster molecules. J. Am. Chem. Soc. 122, 2673-2674 (2000).
- Beecher, A. N. et al. Atomic structures and gram scale synthesis of three tetrahedral quantum dots, J. Am. Chem. Soc. 136, 10645-10653 (2014).
- Kasuya, A. et al. Ultra-stable nanoparticles of CdSe revealed from mass spectrometry. Nat. Mater. 3, 99-102 (2004).
- Jasieniak, J., Smith, L., Embden, J. v., Mulvaney, P. & Califano, M. Re-examination of the size-dependent absorption properties of CdSe quantum dots. J. Phys. Chem. C 113, 19468-19474 (2009).
- Yang, J. et al. Route to the smallest doped semiconductor: Mn²⁺-doped (CdSe)₁₃ clusters. *J. Am. Chem. Soc.* **137**, 12776–12779 (2015).
- Murray, C. B., Kagan, C. R. & Bawendi, M. G. Synthesis and characterization of monodiserse nanocryastals and close-packed nanocrystal assemblies. Annu. Rev. Mater. Sci. 30, 545-610 (2000)
- Ashoori, R. C. Electrons in artificial atoms. Nature **379**, 413-419 (1996).
- Liu, T., Diemann, E., Li, H., Dress, A. W. M. & Müller, A. Self-assembly in aqueous solution of wheelshaped Mo $_{154}$ oxide clusters into vesicles. *Nature* **426**, 59–62 (2003).
- Long, D.-L., Tsunashima, R. & Cronin, L Polyoxometalates: building blocks for functional nanoscale systems. Angew. Chem. Int. Ed. Engl. 49, 1736-1758 (2010).
- Keggin, J. F. Structure of the molecule of 12-phosphotungstic acid. Nature 131, 908-909 (1933)
- Dawson, B. The structure of the 9(18)-heteropoly anion in potassium 9(18)-tungstophosphate,
- $K_6(P_2W_{18}O_{62}) \cdot 14H_2O$. *Acta Cryst.* **6**, 113–126 (1953). Anderson, J. S. Constitution of the poly-acids. *Nature* **140**, 850-850 (1937).
- Khanna, S. N. & Jena, P. Assembling crystals from
- clusters. *Phys. Rev. Lett.* **69**, 1664–1667 (1992). Collier, C. P., Vossmeyer, T. & Heath, J. R. Nanocrystal superlattices. *Annu. Rev. Phys. Chem.* **49**, 371–404 (1998).
- Medeiros-Ribeiro, G., Ohlberg, D. A. A., Williams, R. S. & Heath, J. R. Rehybridization of electronic structure in compressed two-dimensional quantum dot superlattices. Phys. Rev. B 59, 1633-1636 (1999).
- Choi, C. L. & Alivisatos, A. P. From artificial atoms to nanocrystal molecules: preparation and properties of more complex nanostructures. Annu. Rev. Phys. Chem. **61**, 369-389 (2010).
- Cölfen, H. & Antonietti, M. Mesocrystals and Nonclassical Crystallization (Wiley, 2008). De Yoreo, J. J. et al. Crystallization by particle
- attachment in synthetic, biogenic, and geologic environments. Science 349, aaa6760 (2015). This paper introduces various crystallization processes that do not belong to the picture of
- classical crystal growth theory. Larson, R. B. The physics of star formation. *Rep. Prog.* Phys. 66, 1651-1697 (2003).
- Whitesides, G. M. & Grzybowski, B. Self-assembly at all scales. Science 295, 2418-2421 (2002).

- 78. Mullin, J. W. Crystallization 4th edn (Butterworth-Heinemann, 2001).
- Kwon, S. G. & Hyeon, T. Formation mechanisms of uniform nanocrystals via hot-injection and heat-up methods. Small 7, 2685-2702 (2011). Two representative size distribution control methods for monodisperse nanoparticles are fully discussed with experimental evidence and theoretical models.
- Kwon, S. G. *et al.* Kinetics of monodisperse iron oxide nanocrystal formation by "heating-up" process. *J. Am. Chem. Soc.* **129**, 12571–12584 (2007).
- LaMer, V. K. & Dinegar, R. H. Theory, production and mechanism of formation of monodispersed hydrosols. J. Am. Chem. Soc. 72, 4847-4854 (1950).
- Cahn, J. W. On spinodal decomposition. *Acta Mater*. 9, 795-801 (1961).
- Baumgartner, J. et al. Nucleation and growth of magnetite from solution. Nat. Mater. 12, 310-314
 - Conditions for the formation of amorphous nuclei and amorphous-to-crystalline phase transition are discussed in this paper.
- Watzky, M. A. & Finke, R. G. Transition metal nanocluster formation kinetic and mechanistic studies. A new mechanism when hydrogen is the reductant: slow, continuous nucleation and fast autocatalytic surface growth. J. Am. Chem. Soc. 119, 10382-10400 (1997). This study established autocatalytic formation kinetics of nanoclusters with emphasis on the interaction between the precursor and the preformed nanoclusters.
- Fang, J., Ding, B. & Gleiter, H. Mesocrystals: syntheses in metals and applications. *Chem. Soc. Rev.* **40**, 5347-5360 (2011).
- Lu, Y. & Chen, W. Sub-nanometre sized metal clusters: from synthetic challenges to the unique property discoveries, Chem. Soc. Rev. 41. 3594–3623 (2012).
- Yu, J., Patel, S. A. & Dickson, R. M. In vitro and intracellular production of peptide-encapsulated fluorescent silver nanoclusters. Angew. Chem. Int. Ed. Enal. 46, 2028-2030 (2007).
- Kudera, S. et al. Sequential growth of magic-size CdSe nanocrystals. Adv. Mater. 19, 548–552 (2007).
- Dagtepe, P., Chikan, V., Jasinski, J. & Leppert, V. J. Quantized growth of CdTe quantum dots; observation of magic-sized CdTe quantum dots. J. Phys. Chem. C **111**, 14977–14983 (2007).
- Evans, C. M., Guo, L., Peterson, J. J., Maccagnano-Zacher, S. & Krauss, T. D. Ultrabright PbSe magicsized clusters. Nano Lett. 8, 2896-2899 (2008).
- Chen, H. S. & Kumar, R. V. Discontinuous growth of colloidal CdSe nanocrystals in the magic structure. *J. Phys. Chem. C* **113**, 31–36 (2009).
- Yu, Q. & Liu, C. Y. Study of magic-size-cluster mediated formation of CdS nanocrystals: properties of the magic-size clusters and mechanism implication.
- J. Phys. Chem. C 113, 12766–12771 (2009). Zanella, M., Abbasi, A. Z., Schaper, A. K. & Parak, W. J. Discontinuous growth of II–VI semiconductor nanocrystals from different materials. J. Phys. Chem. C 114, 6205-6215 (2010).
- Harrell, S. M., McBride, J. R. & Rosenthal, S. J. Synthesis of ultrasmall and magic-sized CdSe nanocrystals. *Chem. Mater.* **25**, 1199–1210 (2013).
- Kim, B. H. et al. Sizing by weighing: characterizing sizes of ultrasmall-sized iron oxide nanocrystals using MALDI-TOF mass spectrometry. J. Am. Chem. Soc. **135**, 2407–2410 (2013).
- Jensen, K. M. Ø. et al. Mechanisms for iron oxide formation under hydrothermal conditions: an in situ total scattering study. ACS Nano 8, 10704-10714 (2014).
- Gebauer, D., Völkel, A. & Cölfen, H. Stable prenucleation calcium carbonate clusters. *Science* **322**, 1819–1822 (2008).
- Gary, D. C., Terban, M. W., Billinge, S. J. L. & Cossairt, B. M. Two-step nucleation and growth of InP quantum dots via magic-sized cluster intermediates. Chem. Mater. 27, 1432-1441 (2015).
- Peng, Z. A. & Peng, X. Nearly monodisperse and shape-controlled CdSe nanocrystals via alternative routes: nucleation and growth. *J. Am. Chem. Soc.* 124, 3343-3353 (2002).
- 100. Jiang, Z. J. & Kelley, D. F. Role of magic-sized clusters in the synthesis of CdSe nanorods. ACS Nano 4, 1561-1572 (2010).
- 101. Joo, J., Son, J. S., Kwon, S. G., Yu, J. H. & Hyeon, T. Low-temperature solution-phase synthesis of quantum well structured CdSe nanoribbons. J. Am. Chem. Soc. 128, 5632-5633 (2006)

- 102. Yu, J. H. et al. Giant Zeeman splitting in nucleationcontrolled doped CdSe:Mn²⁺ quantum nanoribbons. Nat. Mater. 9, 47–53 (2010).
- 103. Zhang, T. H. & Liu, X. Y. How does a transient amorphous precursor template crystallization. J. Am. Chem. Soc. 129, 13520–13526 (2007).
- 104. Zhang, T. H. & Liu, X. Y. Nucleation: what happens at the initial stage? Angew. Chem. Int. Ed. Engl. 48, 1308–1312 (2009).
- Zhang, T. H. & Liu, X. Y. Multistep crystal nucleation: a kinetic study based on colloidal crystallization. *J. Phys. Chem. B* 111, 14001–14005 (2007).
- Savage, J. R. & Dinsmore, A. D. Experimental evidence for two-step nucleation in colloidal crystallization. *Phys. Rev. Lett.* 102, 198302 (2009).
- Wolde, P. R. t. & Frenkel, D. Enhancement of protein crystal nucleation by critical density fluctuations. *Science* 277, 1975–1978 (1997).
- Nekilov, P. G. The two-step mechanism of nucleation of crystals in solution. *Nanoscale* 2, 2346–2357 (2010).
- Navrotsky, A. Energetic clues to pathways to biomineralization: precursors, clusters, and nanoparticles. Proc. Natl Acad. Sci. USA 101, 12096–12101 (2004).
- Navrotsky, A. Nanoscale effects on thermodynamics and phase equilibria in oxide systems. *ChemPhysChem* 12, 2207–2215 (2011).
- Zhang, H. & Banfield, J. F. Understanding polymorphic phase transformation behavior during growth of nanocrystalline aggregates: insights from TiO₂. J. Phys. Chem. B 104, 3481–3487 (2000).
- 112. Van Santen, R. A. The Ostwald step rule. *J. Phys. Chem.* **88**, 5768–5769 (1984).
- 113. Garvie, R. C. Stabilization of the tetragonal structure in zirconia microcrystals. *J. Phys. Chem.* 82, 218–224 (1978).
- Joo, J. et al. Multigram scale synthesis and characterization of monodisperse tetragonal zirconia nanocrystals. J. Am. Chem. Soc. 125, 6553–6557 (2003).
- 115. Garzón, I. L. & Posada-Amarillas, A. Structural and vibrational analysis of amorphous Au₅₅ clusters. *Phys. Rev. B* 54, 11796–11802 (1996).
- 116. Chen, X., Samia, A. C. S., Lou, Y. & Burda, C. Investigation of the crystallization process in 2 nm CdSe quantum dots. J. Am. Chem. Soc. 127, 4372–4375 (2005).
- 117. Gilbert, B., Huang, F., Zhang, H., Waychunas, G. A. & Banfield, J. F. Nanoparticles: strained and stiff. *Science* 305, 651–654 (2004).
- Masadeh, A. S. et al. Quantitative size-dependent structure and strain determination of CdSe nanoparticles using atomic pair distribution function analysis. Phys. Rev. B 76, 115413 (2007).
- 119. Piepenbrock, M. O. M., Stirner, T., O'Neill, M. & Kelly, S. M. Growth dynamics of CdTe nanoparticles in liquid and crystalline phases. J. Am. Chem. Soc. 129, 7674–7679 (2007).
- 120. Pouget, E. M. et al. The initial stages of templatecontrolled CaCO₃ formation revealed by cryo-TEM. Science 323, 1455–1458 (2009).
- Laven, J. et al. Ion-association complexes unite classical and non-classical theories for the biomimetic nucleation of calcium phosphate. Nat. Commun. 4, 1507 (2013).
- 122. Wang, L. & Nancollas, G. H. Calcium orthophosphates: crystallization and dissolution. *Chem. Rev.* 108, 4628–4669 (2008).
- 123. Weiner, S. & Addadi, L. Crystallization pathways in biomineralization. *Annu. Rev. Mater. Res.* **41**, 21–40 (2011)
- 124. Gower, L. B. Biomimetic model systems for investigating the amorphous precursor pathway and its role in biomineralization. *Chem. Rev.* 108, 4551–4627 (2008).
- 125. Wang, Z., Wang, F., Peng, Y., Zheng, Z. & Han, Y. Imaging the homogeneous nucleation during the melting of superheated colloidal crystals. *Science* 338, 87–90 (2012).
- Huang, F., Zhang, H. & Banfield, J. F. Two-stage crystal-growth kinetics observed during hydrothermal coarsening of nanocrystalline ZnS. *Nano Lett.* 3, 373–378 (2003).
- 127. Zheng, H. *et al*. Observation of single colloidal platinum nanocrystal growth trajectories. *Science* 324, 1309–1312 (2009).
 128. Evans, J. E., Jungjohann, K. L., Browning, N. D. &
- 128. Evans, J. E., Jungjohann, K. L., Browning, N. D. & Arslan, I. Controlled growth of nanoparticles from solution with *in situ* liquid transmission electron microscopy. *Nano Lett.* 11, 2809–2813 (2011).

- 129. Chai, J., Liao, X., Giam, L. R. & Mirkin, C. A. Nanoreactors for studying single nanoparticle coarsening. J. Am. Chem. Soc. 134, 158–161 (2012).
- 130. Yuk, J. M. *et al.* High-resolution EM of colloidal nanocrystal growth using graphene liquid cells. *Science* **336**, 61–64 (2012).
- Liao, H.-G., Cui, L., Whitelam, S. & Zheng, H. Realtime imaging of Pt₃Fe nanorod growth in solution. *Science* 336, 1011–1014 (2012).
- 132. Wang, C., Qiao, Q., Shokuhfar, T. & Klie, R. F. Highresolution electron microscopy and spectroscopy of ferritin in biocompatible graphene liquid cells and graphene sandwiches. *Adv. Mater.* 26, 3410–3414 (2014)
- 133. Li, Z. Y. et al. Three-dimensional atomic-scale structure of size-selected gold nanoclusters. *Nature* 451, 46–49 (2008).
- 134. Scott, M. C. et al. Electron tomography at 2.4-ångström resolution. Nature 483, 444–448 (2012).
- 135. Aert, Ś. V., Batenburg, K. J., Rossell, M. D., Erni, R. & Tendeloo, G. V. Three-dimensional atomic imaging of crystalline nanoparticles. *Nature* 470, 374–377 (2011).
- Park, J. et al. 3D structure of individual nanocrystals in solution by electron microscopy. Science 349, 290–295 (2015).
- 137. Chen, C.-C. et al. Three-dimensional imaging of dislocations in a nanoparticle at atomic resolution. Nature 496, 74–77 (2013).
 138. Rieger, J. et al. Precursor structures in the
- 138. Rieger, J. et al. Precursor structures in the crystallization/precipitation processes of CaCO₃ and control of particle formation by polyelectrolytes. Faraday Discuss. 136, 265–277 (2007).
- 139. Pouget, E. M. et al. The development of morphology and structure in hexagonal vaterite. J. Am. Chem. Soc. 132, 11560–11565 (2010).
- 140. Davis, T. M. et al. Mechanistic principles of nanoparticle evolution to zeolite crystals. Nat. Mater. 5, 400–408 (2006).
- 141. Shields, S. P., Richards, V. N. & Buhro, W. E. Nucleation control of size and dispersity in aggregative nanoparticle growth. A study of the coarsening kinetics of thiolate-capped gold nanocrystals. *Chem. Mater.* 22, 3212–3225 (2010).
- 142. Banfield, J. F., Welch, S. A., Zháng, H., Ebert, T. T. & Penn, R. L. Aggregation-based crystal growth and microstructure development in natural iron oxyhydroxide biomineralization products. *Science* 289, 751–754 (2000).
- 143. Penn, R. L. & Banfield, J. F. Imperfect oriented attachment: dislocation generation in defect-free nanocrystals. *Science* 281, 969–971 (1998).
- nanocrystals. Science **281**, 969–971 (1998). 144. Penn, R. L. & Banfield, J. F. Oriented attachment and growth, twinning, polytypism, and formation of metastable phases: insights from nanocrystalline ${\rm TiO}_2$ Am. Miner. **83**, 1077–1082 (1998).
- 145. Penn, R. L. & Banfield, J. F. Morphology development and crystal growth in nanocrystalline aggregates under hydrothermal conditions: insights from titania. *Geochim. Cosmochim. Acta* 63, 1549–1557 (1999).
- 146. Li, D. *et al.* Direction-specific interactions control crystal growth by oriented attachment. *Science* **336**, 1014–1018 (2012)
- 1014–1018 (2012).
 147. Pacholski, C., Kornowski, A. & Weller, H. Self-assembly of ZnO: from nanodots to nanorods. *Angew. Chem. Int. Ed. Engl.* 41, 1188–1191 (2002).
- 148. Tang, Z., Kotov, N. A. & Giersig, M. Spontaneous organization of single CdTe nanoparticles into luminescent nanowires. *Science* 297, 237–240 (2002).
- 149. Yu, J. H. et al. Synthesis of quantum-sized cubic ZnS nanorods by the oriented attachment mechanism. J. Am. Chem. Soc. 127, 5662–5670 (2005).
- 150. Yuwono, V. M., Burrows, N. D., Soltis, J. A. & Penn, R. L. Oriented aggregation: formation and transformation of mesocrystal intermediates revealed. J. Am. Chem. Soc. 132, 2163–2165 (2010).
- 151. Shanbhag, S. & Kotov, N. A. On the origin of a permanent dipole moment in nanocrystals with a cubic crystal lattice: effects of truncation, stabilizers, and medium for CdS tetrahedral homologues. *J. Phys. Chem. B* 110, 12211–12217 (2006).
- Huis, M. A. v. et al. Low-temperature nanocrystal unification through rotations and relaxations probed by in situ transmission electron microscopy. Nano Lett. 8, 3959–3963 (2008).
- 153. Min, Y., Akbulut, M., Kristiansen, K., Golan, Y. & Israelachvili, J. The role of interparticle and external forces in nanoparticle assembly. *Nat. Mater.* 7, 527–538 (2008).

- 154. Bishop, K. J. M., Wilmer, C. E., Soh, S. & Grzybowski, B. A. Nanoscale forces and their uses in self-assembly. *Small* 5, 1600–1630 (2009).
 155. Batista, C. A. S., Larson, R. G. & Kotov, N. A.
- 155. Batista, C. A. S., Larson, R. G. & Kotov, N. A. Nonadditivity of nanoparticle interactions. *Science* 350, 1242477 (2015). The complexity of nanoparticle interactions is
- discussed in detail in this paper.
 156. Nie, Z. et al. Self-assembly of metal–polymer analogues of amphiphilic triblock copolymers. Nat. Mater. 6, 609–614 (2007).
- 157. Li, M., Schnablegger, H. & Mann, S. Coupled synthesis and self-assembly of nanoparticles to give structures with controlled organization. *Nature* 402, 393–395 (1999).
- Talapin, D. V. et al. Quasicrystalline order in selfassembled binary nanoparticle superlattices. Nature 461, 964–967 (2009).
- 159. Keys, A. S. & Glotzer, S. C. How do quasicrystals grow?
 Phys. Rev. Lett. 99, 235503 (2007).
 160. Tang, Z., Zhang, Z., Wang, Y., Glotzer, S. C. &
- 160. Tang, Z., Zhang, Z., Wang, Y., Glotzer, S. C. & Kotov, N. A. Self-assembly of CdTe nanocrystals into free-floating sheets. *Science* 314, 274–278 (2006).
- Zhang, Z., Tang, Z., Kotov, N. A. & Glotzer, S. C. Simulations and analysis of self-assembly of CdTe nanoparticles into wires and sheets. *Nano Lett.* 7, 1670–1675 (2007).
- 162. Schliehe, C. et al. Ultrathin PbS sheets by twodimensional oriented attachment. Science 329, 550–553 (2010).
- 163. Zherebetskyy, D. et al. Hydroxylation of the surface of PbS nanocrystals passivated with oleic acid. Science 344, 1380–1384 (2014).
- 164. Son, J. S. et al. Large-scale soft colloidal template synthesis of 1.4 nm thick CdSe nanosheets. Angew. Chem. Int. Ed. Engl. 48, 6861–6864 (2009).
- 165. Son, J. S. et al. Dimension-controlled synthesis of CdS nanocrystals: from 0D quantum dots to 2D nanoplates. Small 8, 2394–2402 (2012).
- 166. Son, J. S. et al. Colloidal synthesis of ultrathin two-dimensional semiconductor nanocrystals. Adv. Mater. 23, 3214–3219 (2011).
 167. Yang, J., Son, J. S., Yu, J. H., Joo, J. & Hyeon, T.
- 167. Yang, J., Son, J. S., Yu, J. H., Joo, J. & Hyeon, T. Advances in the colloidal synthesis of two-dimensional semiconductor nanoribbons. *Chem. Mater.* 25, 1190–1198 (2013).
- 168. Liu, Y.-H., Wang, F., Wang, Y., Gibbons, P. C. & Buhro, W. E. Lamellar assembly of cadmium selenide nanoclusters into quantum belts. J. Am. Chem. Soc. 133, 17005–17013 (2011).
- 169. Wang, F. et al. Two-dimensional semiconductor nanocrystals: properties, templated formation, and magic-size nanocluster intermediates. Acc. Chem. Res. 48, 13–21 (2015).
- Lhuillier, E. et al. Two-dimensional colloidal metal chalcogenides semiconductors: synthesis, spectroscopy, and applications. Acc. Chem. Res. 48, 22–30 (2015).
- Ithurria, S., Bousquet, G. & Dubertret, B. Continuous transition from 3D to 1D confinement observed during the formation of CdSe nanoplatelets. *J. Am. Chem.* Soc. 133, 3070–3077 (2011).
- Li, Z. & Peng, X. Size/shape-controlled synthesis of colloidal CdSe quantum disks: ligand and temperature effects. *J. Am. Chem. Soc.* 133, 6578–6586 (2011).
 Chen, D., Gao, Y., Chen, Y., Ren, Y. & Peng, X.
- 173. Chen, D., Gao, Y., Chen, Y., Ren, Y. & Peng, X. Structure identification of two-dimensional colloidal semiconductor nanocrystals with atomic flat basal planes. *Nano Lett.* 15. 4477–4482 (2015).
- planes. Nano Lett. 15, 4477–4482 (2015).
 174. Herrmann, G., Gleiter, H. & Bäro, G. Investigation of low energy grain boundaries in metal by a sintering technique. Acta Metall. 24, 353–359 (1976).
- 175. Ouyang, G., Wang, C. X. & Yang, G. W. Surface energy of nanostructural materials with negative curvature and related size effects. *Chem. Rev.* 109, 4221–4247 (2009).
- Boneschanscher, M. P. et al. Long-range orientation and atomic attachment of nanocrystals in 2D honeycomb superlattices. Science 344, 1377–1380 (2014).
- Sandeep, C. S. S. et al. Epitaxially connected PbSe quantum-dot films: controlled neck formation and optoelectronic properties. ACS Nano 8, 11499–11511 (2014)
- 178. Liao, H.-G. *et al.* Facet development during platinum nanocube growth. *Science* **345**, 916–919 (2014).
- nanocube growth. *Science* **345**, 916–919 (2014). 179. Bergström, L., Sturm, E. V., Salazar-Alvarez, G. & Cölfen, H. Mesocrystals in biominerals and colloidal arrays. *Acc. Chem. Res.* **48**, 1391–1402 (2015).
- Thou, L. & O'Brien, P. Mesocrystals properties and applications. J. Phys. Chem. Lett. 3, 620–628 (2012).

REVIEWS

- Schwahn, D., Ma, Y. & Cölfen, H. Mesocrystal to single crystal transformation of D,L-alanine evidenced by small angle neutron scattering. *J. Phys. Chem. C* 111, 3224–3227 (2007).
- 182. Cölfen, H. & Mann, S. Higher-order organization by mesoscale self-assembly and transformation of hybrid nanostructures. *Angew. Chem. Int. Ed. Engl.* 42, 2350–2365 (2003).
- 183. Wang, Y., He, J., Liu, C., Chong, W. H. & Chen, H. Thermodynamics versus kinetics in nanosynthesis. Angew. Chem. Int. Ed. Engl. 54, 2022–2051 (2015).
- 184. Gu, J., Zhang, Y.-W. & Tao, F. Shape control of bimetallic nanocatalysts through well-designed colloidal chemistry approaches. *Chem. Soc. Rev.* 41, 8050–8065 (2012).
- 185. Fletcher, N. H. Size effect in heterogeneous nucleation. J. Chem. Phys. 29, 572–576 (1958).
- 186. Winkler, P. M. et al. Heterogeneous nucleation experiments bridging the scale from molecular ion clusters to nanoparticles. Science 319, 1374–1377 (2008).
- Pruppacher, H. R. & Klett, J. D. Microphysics of Clouds and Precipitation (Kluwer, 1997).
- 188. Reiss, P., Protière, M. & Li, L. Core/shell semiconductor nanocrystals. Small 5, 154–168 (2009).
- 189. Zhong, X., Xie, R., Zhang, Y., Basché, T. & Knoll, W. High-quality violet- to red-emitting ZnSe/CdSe core/ shell nanocrystals. *Chem. Mater.* 17, 4038–4042 (2005).
- 190. Kwon, S. G. et al. Heterogeneous nucleation and shape transformation of multicomponent metallic nanostructures. Nat. Mater. 14, 215–223 (2015). Heterogeneous nucleation kinetics of nanoparticles and their nucleation-induced structural changes are studied.

- 191. Ithurria, S., Guyot-Sionnest, P., Mahler, B. & Dubertret, B. Mn²⁺ as a radial pressure gauge in colloidal core/shell nanocrystals. *Phys. Rev. Lett.* 99, 265501 (2007).
- Jesser, W. A. & Kuhlmann-Wilsdorf, D. On the theory of interfacial energy and elastic strain of epitaxial overgrowths in parallel alignment on single crystal substrates. *Phys. Stat. Sol.* 19, 95–105 (1967).
 Matthews, J. W. & Blakeslee, A. E. Defects in epitaxial
- 193. Matthews, J. W. & Blakeslee, A. E. Defects in epitaxia multilayers. I. Misfit dislocations. *J. Cryst. Growth* 27, 118–125 (1974).
- 194. Smith, A. M., Mohs, A. M. & Nie, S. Tuning the optical and electronic properties of colloidal nanocrystals by lattice strain. *Nat. Nanotechnol.* 4, 56–63 (2009).
- lattice strain. Nat. Nanotechnol. 4, 56–63 (2009).

 195. Grünwald, M., Lutker, K., Alivisatos, A. P., Rabani, E. & Geissler, P. L. Metastability in pressure-induced structural transformations of CdSe/ZnS core/shell nanocrystals. Nano Lett. 13, 1367–1372 (2013).
- Tolbert, S. H. & Alivisatos, A. P. The wurtzite to rock salt structural transformation in CdSe nanocrystals under high pressure. J. Chem. Phys. 102, 4642–4656 (1995).
- 197. Strasser, P. et al. Lattice-strain control of the activity in dealloyed core–shell fuel cell catalysts. Nat. Chem. 2, 454–460 (2010).
- 198. Zhang, S. et al. Tuning nanoparticle structure and surface strain for catalysis optimization. J. Am. Chem. Soc. 136, 7734–7739 (2014).
- Moseley, P. & Curtin, W. A. Computational design of strain in core–shell nanoparticles for optimizing catalytic activity. *Nano Lett.* 15, 4089–4095 (2015).
 Brokman, A. & Balluffi, R. W. Coincidence lattice
- Brokman, A. & Balluffi, R. W. Coincidence lattice model for the structure and energy of grain boundaries. *Acta Mater.* 29, 1703–1719 (1981).
- Trampert, A. & Ploog, K. H. Heteroepitaxy of largemisfit systems: role of coincidence lattice. *Cryst. Res. Technol.* 35, 793–806 (2000).

- 202. Kwon, K. W. & Shim, M. _Y-Fe₂O₃/II–VI sulfide nanocrystal heterojunctions. *J. Am. Chem. Soc.* **127**, 10269–10275 (2005).
- Buonsanti, R. et al. Seeded growth of asymmetric binary nanocrystals made of a semiconductor TiO₂ rodlike section and a magnetic ₂-Fe₂O₃ spherical domain. J. Am. Chem. Soc. 128, 16953–16970 (2006).
- 204. Mokari, T., Rothenberg, E., Popov, I., Costi, R. & Banin, U. Selective growth of metal tips onto semiconductor quantum rods and tetrapods. *Science* **304**, 1787–1790 (2004).
- Mokari, T., Sztrum, C. G., Salant, A., Rabani, E. & Banin, U. Formation of asymmetric one-sided metal-tipped semiconductor nanocrystal dots and rods. *Nat. Mater.* 4, 855–863 (2005).
 Zhang, J., Tang, Y., Lee, K. & Ouyang, M. Nonepitaxial
- 206. Zhang, J., Tang, Y., Lee, K. & Ouyang, M. Nonepitaxial growth of hybrid core–shell nanostructures with large lattice mismatches. *Science* 327, 1634–1638 (2010).
- Gu, H., Zheng, R., Zhang, X. & Xu, B. Facile one-pot synthesis of bifunctional heterodimers of nanoparticles: a conjugate of quantum dot and magnetic nanoparticles. J. Am. Chem. Soc. 126, 5664–5665 (2004).
- Buck, M. R., Bondi, J. F. & Schaak, R. E. A totalsynthesis framework for the construction of high-order colloidal hybrid nanoparticles. *Nat. Chem.* 4, 37–44 (2012).
- 209. Wu, H. et al. Formation of heterodimer nanocrystals: UO_2/ln_2O_3 and $FePt/ln_2O_3$. J. Am. Chem. Soc. 133, 14327-14337 (2011).

Acknowledgements

This work was supported by the Institute for Basic Science (IBS) in Republic of Korea (IBS-R006-D1 and IBS-R006-Y1).

Competing interests statement

The authors declare no competing interests.